

Linköping Studies in Science and Technology
Dissertations No. 2292

Multifunctional Nanocellulose Composite Materials

Olof Eskilson

Linköping Studies in Science and Technology.
Dissertation No. 2292

Multifunctional Nanocellulose Composite Materials

Olof Eskilson



Division of Biophysics and Bioengineering (BBIOBIO)
Department of Physics, Chemistry and Biology (IFM)
Linköping University, SE-581 83 Linköping, Sweden
Linköping 2023

Cover: Scanning electron microscopy micrographs of BC-AuNP cross section (front, bottom right corner) and of BC (front, top left corner). Back cover shows a light microscopy image of BC-AuNP.

During the course of the research underlying this thesis, Olof Eskilson was enrolled in Forum Scientium, a multidisciplinary doctoral program at Linköping University, Sweden.

© Copyright 2023 Olof Eskilson



This work is licensed under a Creative Commons Attribution 4.0 International License.

Eskilson, Olof
Multifunctional Nanocellulose Composite Materials
ISBN 978-91-8075-061-5 (print)
ISBN 978-91-8075-062-2 (PDF)
<https://doi.org/10.3384/9789180750622>
ISSN 0345-7524

Printed in Sweden by LiU-Tryck, 2023

Abstract

Nanoparticles (NPs) are particles with more than one dimension between 1 and 100 nm. Because of their small size, they typically display different physical and chemical properties than the corresponding bulk materials. NPs have been used in many different applications, such as in electronics, optics, catalysis, and in biomedicine. Due to their colloidal nature, NPs are often immobilized on a solid substrate, such as glass or polymer-based materials, including biopolymers. Nanocellulose is a biopolymer-based nanomaterial that can be obtained from plants or bacterial biofilms. They can be processed into thin and highly hydrated films with high mechanical strength and can serve as a versatile substrate for NPs. Bacterial cellulose (BC) is also an interesting material for generating wound dressings. The combination of NPs and BC results in soft and flexible nanocomposites (BC-NPs) that can demonstrate novel properties and improve the functionality of wound dressings.

BC-NP nanocomposites have previously been obtained by impregnating BC with the reactants needed for synthesis of the NPs and allowing the reaction to proceed *in situ*, inside and on the surface of the BC. This strategy limits the possibilities to control NP geometry and NP concentration and make synthesis of nanocomposites with more sophisticated compositions very challenging. In addition, the synthesis conditions used can potentially have negative effects on the properties of BC.

The work presented in this thesis shows the possibility to produce well-defined, tunable BC-NP nanocomposites using self-assembly under very benign conditions that enable functionalization of BC with a wide range of different types of NPs. In addition to exploring the self-assembly process and the physical properties of these new BC-NP composites, several different applications were investigated. The functionalization of BC with gold nanoparticles (AuNPs) of different sizes and geometries was demonstrated. The resulting materials were used for development of a new sensor transduction technology, exploiting the optical response upon mechanical compression to detect biomolecules. BC-AuNP nanocomposites were also developed for monitoring of protease activity of wound pathogens, for catalysis, and for fabrication of ultra-black materials with unique absorption and scattering profiles of light in the visible and near infrared spectral range. In addition, the self-assembly process could be adopted for generating BC-mesoporous silica nanoparticles (MSNs) nanocomposite wound dressings. The resulting high surface area materials could be used as carriers for pH sensitive dyes. The pH-responsive BC-MSNs demonstrated adequate biocompatibility and allowed for monitoring of wound pH and for assessment of wound status.

The strategies for functionalization of BC with inorganic NPs that was developed and explored in this thesis are highly versatile and allow for fabrication of a wide range of multifunctional nanocomposite materials.

Populärvetenskaplig sammanfattning

Människan har i alla tider försökt utveckla processer och verktyg för att förbättra sina livsbetingelser på jorden. Nu, när tekniska framsteg har gjort det möjligt att designa och tillverka material på nanonivå expanderar möjligheterna för nya innovationer. Till exempel går det att kombinera olika material på nanonivå till kompositer med flera funktioner och egenskaper som är ouppnåeliga med de involverade materialen var för sig. Sådana multifunktionella kompositer har tillämpats inom en rad olika områden som sjukvård, mätteknik och katalys. Nanopartiklar med olika egenskaper har uppmärksammats som intressanta kandidater till sådana kompositer. Vanligtvis används de tillsammans med ett strukturmateriel, ofta någon typ av cellulosa, för att hålla partiklarna på plats – något som underlättar och expanderar möjligheterna för deras användning vid olika tillämpningar. Partikeltyperna som används är flera, till exempel har metalliska partiklar av guld och silver optiska egenskaper som gör dem lämpade för användning i sensorer. Även keramiska partiklar, som med sin stora ytaarea passar för tillämpningar inom vattenrening eller i läkemedelsformuleringar, har använts.

I denna avhandling presenteras ett nytt sätt att kombinera nanopartiklar med bakteriell nanocellulosa genom självorganisation. Självorganisation innebär att materialen spontant associerar och bildar nya strukturer och material vid vissa precisa och väldefinierade betingelser. Detta tillvägagångssätt tillåter stor flexibilitet i skapandet av nanokompositer och leder till material med förbättrade och nya, intressanta, egenskaper. Eftersom bakteriell nanocellulosa uppvisat mycket goda egenskaper i avancerade sårförband har kompositernas egenskaper som funktionella sårvårdsmaterial undersökts. Även kompositer med nya egenskaper för sensorer, katalysatorer, och ljusabsorberande material har studerats.

Resultaten visar att koncentrationen av joner vid tillverkningen är avgörande för självorganiseringsprocessen. Processen fungerar för nanopartiklar av olika typer: metalliska guld- och silverpartiklar med olika storlekar och geometriska former; samt porösa keramiska kiseldioxidpartiklar. Dessutom ger processen god kontroll över partikelkoncentrationen i kompositerna, något som användes för att tillverka kompositer med mycket stort antal partiklar, vilket resulterade i hög ljusabsorptans. En ny typ av guldpartikel-baserad sensor som reagerar på tryck har tagits fram och ytterligare funktionalisering resulterade i en nanokomposit med möjligheten att påvisa förekomsten av bakterier. Detta kan användas för att snabb detektion av infektioner i sår. För samma ändamål har ett pH-känsligt material tagits fram genom att kombinera porösa kiseldioxidpartiklar och bakteriell nanocellulosa. Guldnanopartiklar har goda katalytiska egenskaper och den stora ytan i förhållande till volym av partiklarna tenderar att resultera i effektiv katalys. I en kombination med bakteriell nanocellulosa uppnåddes hög katalytisk effekt, samtidigt som guldnanopartiklarnas kolloidial stabilitet upprätthölls. Sammantaget visar avhandlingen att metoden som utvecklats för tillverkning av nanokompositer är mycket kraftfull och kan användas för tillverkning av material med många nya egenskaper och användningsområden.

List of publications

This thesis is based on the following publications:

Paper I

Self-Assembly of Mechanoplasmonic Bacterial Cellulose-Metal Nanoparticle Composites

Eskilson O., Lindström S.B., Sepulveda B., Shahjamali M.M., Güell-Grau P., Sivilér P., Skog M., Aronsson C., Björk E.M., Nyberg N., Khalaf H., Bengtsson T., James J., Ericson M.B., Martinsson E., Selegård R., and Aili D.

Advanced Functional Materials **2020**, 30, 2004766

Author's contribution:

O.E. synthesized the BC-NP composites, planned, and performed mechanoplasmonic and refractometric experiments. O.E. performed the modelling of S/N and wrote the simulation script. O.E. drafted the manuscript. S.B.L. performed the BC-AuNP potential interaction simulations.

Paper II

Nanocellulose Composite Wound Dressings for Real-Time pH Wound Monitoring

*Eskilson O.**, Zattarin E.*, Berglund L., Oksman K., Hanna K., Rakar J., Sivilér P., Skog M., Rinklake I., Shamasha R., Sotra Z., Starkenberg A., Odén M., Wiman E., Khalaf H., Bengtsson T., Junker J.P.E., Selegård R., Björk E.M., and Aili D.

* *Equal contribution*

Submitted (2023)

Author's contribution:

O.E, together with E.Z., synthesized the pH@BC composites, planned experiments, and drafted the manuscript. E.M.B synthesized the nanoparticles and conducted the nitrogen physisorption experiments.

Paper III

Bacterial Cellulose–Gold Nanoparticle Composite Wound Dressings for Protease Activity Monitoring

Eskilson O., Wiman E., Reustle N., Sotra Z., Svärd A., Junker J.P.E., Khalaf H., Bengtsson T., Selegård R., and Aili D.

In Manuscript (2023)

Author's contribution:

O.E. synthesized the BC-AuNP composites, planned, and performed the fluorescence recovery experiments and drafted the manuscript. R.S. and N.R. synthesized the polypeptides, and O.E together with N.R. conducted the polypeptide fluorescence recovery experiments.

Paper IV

Self-Assembled Nanocellulose–Metal Nanoparticle Composites for Catalysis

Eskilson O., Kollenchery Ramanathan S., Selegård R., and Aili D.

In Manuscript (2023)

Author's contribution:

O.E. and S.K.R. planned and performed the experiments. O.E drafted the manuscript.

Paper V

Ultra-black Nanocellulose–Gold Nanoparticle Composites

Eskilson O., Silander J., Hallberg T., Åkerlind C., Järrendahl K., Selegård R. and Aili D.

In Manuscript (2023)

Author's contribution:

O.E. synthesized the AuNPs and the BC-AuNP composites. O.E, J.S. and T.H performed the optical measurements. O.E. drafted the manuscript.

Papers not included in the thesis

Paper VI

Real-time Nanoplasmonic Sensor for IGG monitoring in Bioproduction

Tran T., Eskilson O., Mayer F., Gustavsson R., Selegård R., Lundström I., Mandenius C.-F., Martinsson E., and Aili D.

Processes **2020**, 8, 1-12

Paper VII

Elastic Plasmonic-Enhanced Fabry-Pérot Cavities with Ultrasensitive Stretching Tunability

Güell-Grau P., Pi F., Villa R., Eskilson O., Aili D., Nogués J., Sepúlveda B., and Alvarez M.

Advanced Materials, **2022**, 34, 2106731

Abbreviations

| | |
|--------|-------------------------------------|
| 4NP | 4-nitrophenol |
| AuNP | Gold nanoparticle |
| AuNR | Gold nanorod |
| BC | Bacterial cellulose |
| BSA | Bovine serum albumin |
| CNC | Cellulose nanocrystal |
| Col-1 | Collagenase I |
| CTAB | Cetyltrimethylammonium bromide |
| FOM | Figure of merit |
| FWHM | Full-width-half-maximum |
| LbL | Layer-by-layer |
| LSPR | Localized surface plasmon resonance |
| MMP | Matrix metalloproteinase |
| MSN | Mesoporous silica nanoparticle |
| NP | Nanoparticle |
| NS | Nanostructure |
| PEI | Polyethyleneimine |
| PMMA | Poly(methyl methacrylate) |
| RI | Refractive index |
| SEM | Scanning electron microscopy |
| SPR | Surface plasmon resonance |
| UV-vis | Ultraviolet-visible |

Acknowledgements

I would like to extend my warmest thanks to my supervisor **Daniel**, for believing in me enough to take me on as your PhD student. For your contagious love of science and for your guidance through these 4 plus years. I am proud of the work that we have accomplished together.

A heartfelt thank you also to my co-supervisor **Robert**, for being the rock in the storm that the graduate studies ultimately are. I think I speak for the entirety of M2Lab when I say that your great kindness and helpfulness is a blessing to us all. We owe you a lot.

Thanks also to my other co-supervisor, **Erik**, for your excellent guidance in the early days of my studies, and for always having good answers for any plasmonics related question.

To all the present and past **colleagues of M2Lab**, for all the fun times we have had and for our shared frustration when things go wrong in the lab, thank you.

Thanks also to everyone in the **HEALiX team**, what a great bunch you are. It has been a pleasure to work with you all and get to know you. To all my collaborators at IFM and LiU, **Emma** and **Stefan**, and to all other collaborators inside and outside of Sweden.

Thanks to my office mates, **Béla, Mike, Philip, Alexandra** and **Sneha**, for making work a bit more fun and for all our interesting discussions.

To the people at our lunch table, the rest of the people in the division of biophysics and bioengineering and molecular surface physics and nanoscience and to past members of the **Kaffeklubb**. You have made IFM a wonderful working place, thank you.

Thanks also to all my lovely friends, near and far who have cheered me on throughout this journey. Your support has been invaluable. **Karin, Jimmy, Tilda, Jakob, Jonas, Sofia, Oskar, Jennifer** and many more. Thank you!

Thanks to everyone who rally for (most) Thursday quiz at ÅGB, you have helped me keeping my spirits high these last few years.

And last but not least, to my **family**, for always taking an interest in what I am doing (even though you always forget) and for supporting me unconditionally, thank you.

1

| | |
|---------------------------|----------|
| Introduction | 3 |
| Nanocomposites..... | 4 |
| Aim | 5 |
| Thesis Outline | 5 |

2

| | |
|--|----------|
| Nanoparticles..... | 7 |
| Surface and size effects | 7 |
| Colloids..... | 9 |
| Plasmonic properties of metallic nanoparticles | 11 |
| Nanoparticles for catalysis..... | 16 |

3

| | |
|---|-----------|
| Substrates for nanoparticle immobilization | 19 |
| Two-dimensional substrates..... | 19 |
| Bacterial cellulose | 20 |
| Bacterial cellulose as a wound dressing material..... | 24 |

4

| | |
|---|-----------|
| Synthesis and application of BC-nanoparticle composites | 27 |
| State of the art..... | 27 |
| Self-assembly of citrate stabilized AuNPs to BC | 29 |
| Mechano- and thermoplasmonic properties | 33 |
| Broadband adsorbing properties of self-assembled BC-AuNP composites | 35 |
| Catalytic properties of self-assembled BC-NP composites | 37 |
| BC-NP composites for advanced wound care..... | 38 |

5

| | |
|--------------------------------|-----------|
| Summary of papers | 43 |
| Paper I | 44 |

| | |
|--|-----------|
| Paper II..... | 45 |
| Paper III | 46 |
| Paper IV..... | 47 |
| Paper V | 48 |
| 6 | |
| Conclusions and future outlook..... | 49 |
| References..... | 53 |

Introduction

Humans have made deliberate use of nanomaterials for thousands of years. At such an early time point in human history, the nanoscale nature of the materials was unknown, but their properties made them attractive for several uses, most often as dyes for luxurious ceramics and glassware. Ancient civilizations in Mesopotamia and Egypt learned to synthesize these materials and the Lycurgus cup stands as a famous example from 4th century Roman era, which uses silver and gold nanoparticles (NPs) for impressive optical effects.^[1] Later, drinkable gold was hailed as an elixir of longevity and used in medicine for a number of ailments such as leprosy, diarrhea and epilepsy.^[2,3] Additionally, gold NPs were widely used in rose glass for church windows from early medieval times up to today.^[4]

NPs are defined by the EU commission as “a small piece of matter of defined physical boundaries” where “one or more external dimensions are in the size range of 1 nm to 100 nm”.^[5] NPs of natural origin are common, such as dust created from weathering of rock, or soot from volcanic eruptions and they are ubiquitous and abundant in our

surroundings. Since the start of the industrial era, human made processes have unintentionally added vast amounts of NPs to our environment through energy production, mining and from everyday life activities such as driving a car.^[6]

It was not until 1856 when Michael Faraday synthesized a gold NP colloid that the color was identified to be the result of minute pieces of metallic gold.^[7] Around half a century later, Gustav Mie successfully gave a scientific explanation for the vibrant colors of metallic NPs.^[8] There are effects, other than sometimes their striking optical properties, that arise due to the small size of NPs. When materials are miniaturized, their surface to volume ratio increases dramatically, and when transitioning from microscale to nanoscale, surface to volume ratio increases three orders of magnitude causing surface effects to often dominate nanoscale interactions.^[9]

During the decades following Mie's discovery, nanosized materials and their applications gathered increasing interest and the knowledge of how to purposefully design and synthesize nanomaterials has been rising steadily. This has allowed the creation of nanocomposites where two or more nanoscale materials have been combined in order to achieve properties unobtainable by the constituent materials on their own.^[9] Macroscale composites have been used by humans for a long time, for example by combining straw and mud for bricks, or the more modern use of concrete and steel to form reinforced concrete for construction. In later years, the use of nanocomposites based on different types of nanostructures (NS) has been increasing. NSs such as carbon nanotubes and metallic or ceramic NPs, has found use in a wide range of applications such as electronics,^[10–12] sensing,^[13] biomedicine,^[14,15] material reinforcement,^[16–18] energy harvesting,^[19] packaging,^[20] and catalysis.^[21–23]

Nanocomposites

Due to their colloidal nature, many applications of NPs benefit from immobilization of NPs on a solid support. Immobilization, for example, allows for changing the surface chemistry of NPs without having to worry about maintaining colloidal stability. Common substrates for immobilization of NPs are glass or polymer-based substrates, including biopolymers. Bacterial cellulose (BC) is a biopolymer that has been gaining

significant interest as a material for fabrication of nanocomposites due to its nanoscale fibrillar structure, interesting mechanical properties, and low toxicity. BC has also been successfully used as a wound dressing material for burns and hard to heal wounds due to its conformability to skin, permeability to gases and high water content that promote moist wound healing. Most BC-based nanocomposites have been obtained by synthesis of NPs *in situ* through reduction of metal salts, either by BC alone or by addition of various reducing agents. The resulting materials typically show NPs bound to BC fibrils. However, *in situ* synthesis strategies are typically difficult to tailor and provide limited possibilities to control NP geometry, composition, and NP concentration.

Aim

The aim of the work presented in this thesis was to explore the possibilities of fabricating multifunctional BC-NP nanocomposites through self-assembly. Both the factors affecting the self-assembly process and the nature of the interactions between NPs and BC, as well as the properties of the resulting nanocomposites were investigated. Moreover, various applications relating to sensing, catalysis, and wound diagnostics were explored.

Thesis Outline

The thesis is based on five papers, which all include BC-NP nanocomposites. In **Paper I** we show the possibility of producing BC-NPs by self-assembly and describe the underlying forces driving the BC-NP interactions. We show that the strategy applies to gold NPs (AuNPs) of different geometries as well as spherical silver NPs (AgNPs). The BC-AuNP nanocomposites were then used for development of a novel mechanoplasmonic transduction technology. The materials also showed enhanced refractometric performance in comparison to standard two-dimensional glass substrates. In **Paper II** we showed that a similar self-assembly strategy could be used for ceramic mesoporous silica nanoparticles (MSNs) to create nanocomposites with very high specific surface area. These materials were then used to adsorb a pH-responsive dye to create wound dressing sensors that can visually indicate the pH value in a wound. Wound pH correlates with infections and the pH-responsive wound

dressings can hence potentially be used for wound diagnostics. **Paper III** also focused on a sensor for detection of wound infections but instead used proteases as a biomarker for wound status. A fluorophore-labelled protease substrate (polypeptide) was immobilized on AuNPs adsorbed in the BC. The short distance between the AuNP and the fluorophores led to quenching. The cleavage of the polypeptide by proteases from common wound pathogens resulted in a significant increase in fluorescence. In **Paper IV** we exploited the tunable NP self-assembly process to create BC-AuNP nanocomposites with very high densities of AuNPs for catalysis. A model reaction based on the reduction of 4-nitrophenol (4NP) by sodium borohydride was used to study the catalytic properties of the nanocomposites. In **Paper V** we explored possibilities to further maximize the amount of AuNPs in the BC-AuNP nanocomposites to create materials that scatter and absorb electromagnetic radiation with high efficiency, in a facile and inexpensive synthesis procedure. The materials retained the flexible properties of BC after functionalization.

Nanoparticles

Surface and size effects

A surface is the boundary of a material and the amount of surface and its properties play an important role in the behavior of a system. When decreasing the size of a particle, the surface decreases with r^2 while the volume decreases with r^3 . Since the volume decreases much faster than the surface area, nano-sized particles will have a large surface to volume ratio.^[24]

For porous materials, understanding the effects of large surface area is of utmost importance to understand their properties. Porous materials can be made in macroscopic size but may have nanoscale cavities, pores, to achieve huge specific surface areas. These materials are classified depending on the size of their pores where materials with <2 nm diameter pores are called microporous, 2–50 nm mesoporous, and materials with pores above 50 nm are called macroporous.^[25–27] The choice of base

material is commonly some type of ceramic material with either very well-defined crystal structures, like naturally occurring microporous zeolite, for instance aluminosilicate, or materials partially lacking crystal structure, like amorphous mesoporous silica (SiO_2). These materials have found much use in sorption applications, for example as molecular sieves where pore size and geometry constraints can cause adsorption of specific molecules in a solution, or for catalysis, either as catalyst support or active catalysts.^[22,28–30]

Furthermore, mesoporous silica can be made into nanoparticles, MSNs, of different sizes containing pores of roughly 3–12 nm diameter, expanding their potential use.^[31] These have been used in several applications such as drug delivery,^[32] catalysis,^[33,34] and gas sensing.^[35,36]

Surface atoms have fewer atom neighbors that bind and stabilize them than bulk atoms. The number of neighbours an atom interacts with is called *coordination number*, and surface atoms therefore have lower coordination number than their bulk counterparts. Lowest coordinated atoms of NPs are found on sharp corners, followed by the edge of the NP, the surface, and lastly, bulk atoms, which show the highest coordination number in the system. The strength and nature of inter-atomic forces of the material decides the resulting inward force from the bulk atoms on the surface atoms and give rise to surface tension, or surface energy in the material.^[37] Surface tension has been shown to be lower in systems with lower mean coordination.^[38] Additionally, since the melting point is directly correlated to the amount of energy required to break the inter-atomic bonds of the material, melting points in low-coordinated systems are generally lower than for high-coordination systems. However, at sufficiently small NP sizes, classically defined phase transitions break down and it is no longer possible to tell one phase from the other.^[24]

Low coordination also leaves atomic orbitals unsatisfied, causing surface atoms to interact with atoms and molecules in their vicinity to which their bulk counterpart would be inert. Systems with low mean coordination are hence much more reactive than high coordination systems like macroscopically sized materials, and systems

containing small NPs have shown great increase in catalytic activity in comparison to systems with larger NPs.^[39–42]

Colloids

Solid particles suspended in a liquid phase form a colloid. Colloids of NPs are often created through a nucleation of metals salts dissolved in an aqueous phase. Nucleation is when a concentrated solvent is separating from the solution phase due to supersaturation, forming a solid phase.^[43] The nucleus will successively grow larger as more and more atoms coalesce to form a particle with a final size dependent on the amount of solubilized metal ions. The number of particles and their respective size is hence a result of the total amount of nucleations occurring during synthesis and the available metal ions. The nucleation can also occur at so-called *nucleation sites*, such as at vessel surface defects or at impurities present in the solution.^[44–46] This process is exploited in seed-mediated synthesis where small, well-defined NPs are added to act as nucleation sites, offering a way to control synthesis parameters, for example growth direction. The seeds are synthesized via reduction of metal salts.^[47–50] The seeds are then added in a known number to a solution containing metal salts and a reducing agent and in some cases additional additives to drive growth in a specific direction. The seeds will be the primary nucleation sites and final NP concentration and shape can thus be tightly controlled, while the concentration of metal salts will determine the final size of the NPs.^[48,51,52] The Turkevich method, which yields relatively monodisperse NPs using citrate as both reduction agent and stabilizer, is one of the most widely used techniques for synthesizing AuNPs.^[53,54]

After or during synthesis, the NPs are usually dispersed in aqueous media. To prevent or limit processes that would compromise the performance of the NPs, such as Ostwald ripening, flocculation, and aggregation, the particles are synthesized in a way that also provide sufficient colloidal stability.^[55] This can be accomplished by adsorption of species to, or functionalization of, the NP surface that can provide sufficient repulsion between NPs to delay or prevent strong NP-NP interactions.^[54] Properly stabilized colloids can remain in suspension for a very long time, sometimes up to hundreds of years as in the case of some of Faraday's AuNP colloids, which were made in 1856 and

are still on display at The Royal Institution, London. Another way of stabilizing NPs is by functionalizing the surface with a polymer. Polymers can prevent the interparticle distance from becoming too small through their presence alone, thereby sterically stabilizing the colloid.^[56–58] More commonly, repulsion is created through the introduction of charges by adsorbing ionic species, for example citrate or charged surfactants like cetyltrimethylammonium bromide (CTAB) to the metal surface.^[51,52,59–61]

Due to the surface energy of a NP, ions readily adsorb to the metal surface, leading to a buildup of charge depending on the surface chemistry and available ions. The ions extend some distance into the bulk where counterions amass to neutralize the adsorbed ions. The counterions electrostatically further attract ionic species until what is called a diffuse electric double-layer has formed, with a thickness depending on the colloidal species, the ionic strength of the medium, the available ions and temperature. The first layers of ions are strongly attached to the NP and less frequently exchanged, they form the Stern layer and have water molecules oriented and strongly attached. The size of the NP and the associated water is sometimes referred to as the hydrodynamic radius (Figure 2.1).^[62]

The potential at the slipping plane is called ζ (Zeta)-potential. This can be measured using different techniques and gives an indication of colloidal stability and interaction with other charges species. Colloids exhibiting large negative (usually around -30 mV >) or large positive (30 mV <) ζ -potentials are deemed fairly colloidally stable when considering charge alone. For this reason, charge stabilized colloids are sensitive to concentration of ionic species in the colloid medium and may become unstable with increasing ionic strength. Additionally, since the ζ -potential of citrate-capped NPs arises due to carboxyl-groups on the citrate molecule, changes in pH will affect the ζ -potential and subsequently, the stability. Using this knowledge, it is possible to tune the colloidal stability by changing ionic strength or pH to selectively adsorb NPs to substrates while maintaining repulsion and stability between the NPs.^[63,64] This can be used to synthesize NP-composites with control over NP concentration and interparticle

spacing to tune the resulting composite properties, a phenomenon exploited in **Paper I**.

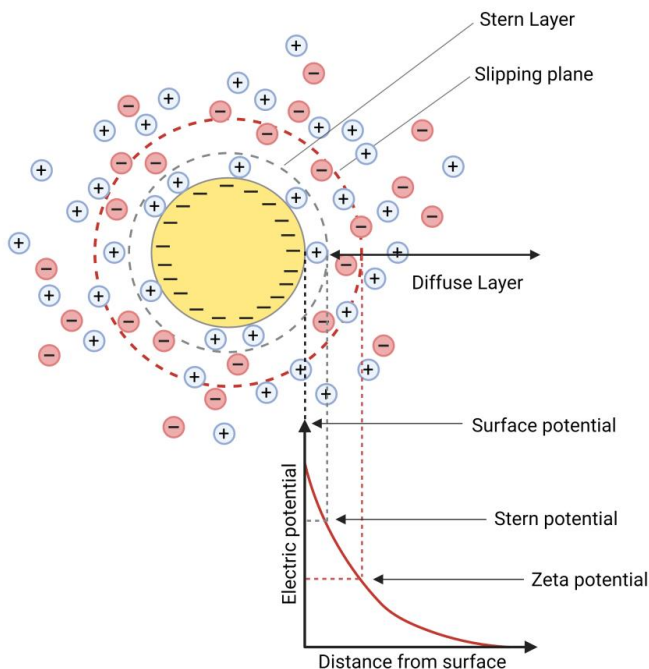


Figure 2.1: Schematic representation of the ion distribution surrounding a solid in aqueous solution.

Plasmonic properties of metallic nanoparticles

In 1908 Mie described how metal nanoparticles interact with light by solving the Maxwell equations for small metallic spheres.^[8] His work showed that when materials are made sufficiently small, nanoscale effects will dominate their physical properties. When a metal particle is smaller than about half the wavelength (λ) of light, the NP experiences the electric field of the incident light homogeneously over the entire particle resulting in collective oscillation of the free electrons in the NP metal lattice. This phenomenon is called localized surface plasmon resonance (LSPR), where absorbed light induces movement in the electron gas of metallic nanoparticles. Plasmons are thus density oscillations in the electron gas of a metal and can occur in metals of any shape or size.^[65]

Unlike surface plasmon resonance (SPR) in macroscopic metal interfaces, where both energy and momentum of the incident light must match the excited surface plasmon polariton to incite propagation,^[66,67] electron movement in NPs is so confined to the limited geometry that plasmons cannot propagate. This has the effect that simply matching excitation energy is sufficient to induce localized electron oscillation in NPs.^[68,69] Hence, LSPR requires less sophisticated optics and allows miniaturization of LSPR-based instruments.^[70]

How materials interact with electromagnetic radiation is in large dependent on a material property called permittivity, denoted ϵ . For a spherical metal NP with radius much smaller than the wavelength of the incident light ($2r \ll \lambda$), the optical cross section can be expressed as:^[71,72]

$$\sigma_{ext}(\lambda) = \frac{24\pi^2 r^3 \epsilon_d^{3/2} N}{\lambda \ln(10)} \frac{\epsilon_i(\lambda)}{(\epsilon_r(\lambda) + 2\epsilon_d)^2 + \epsilon_i(\lambda)^2} \quad (2.1)$$

Where r is the radius of the NP, ϵ_d is the permittivity of the surrounding medium, ϵ_r and ϵ_i are the real and imaginary parts of the complex permittivity for the bulk metal, respectively, and N is the electron density. In the timeframe of light propagation, NP is taken to be stationary and subject to a non-changing, homogeneous electric field (quasistatic). The NP can therefore be considered an electrical dipole and its polarizability (α) can be described as:

$$\alpha(\lambda) = 4\pi r^3 \frac{\epsilon(\lambda) - \epsilon_d(\lambda)}{\epsilon(\lambda) + 2\epsilon_d(\lambda)} \quad (2.2)$$

Here, ϵ is the relative permittivity of the metal NP. From this relation, it follows that maximum polarization is reached when the denominator is as small as possible (i.e., when $\epsilon(\lambda) \approx -2\epsilon_d(\lambda)$). From equation 2.1, maximum absorptive cross section is reached when this requirement is fulfilled and plasmon resonance arises.

By using the Drude model for calculating the metal permittivity we see that:^[73]

$$\epsilon_{\text{Drude metal}}(\omega) = 1 - \frac{\omega_p^2}{\omega^2 + i\omega\gamma} \quad (2.3)$$

And the resonance frequency is given by:

$$\omega_0 = \frac{\omega_0}{\sqrt{1 + 2\epsilon_d}} \quad (2.4)$$

Which shows that the frequency will decrease, and the plasmon resonance redshift, as the relative permittivity of the surrounding increases. The electrons of the NPs are displaced upon fulfillment of the resonance criteria and will oscillate similarly to a damped harmonic oscillator. The restoring force in the case of a metal NP undergoing plasmon resonance are the stationary, positively charged atomic nuclei, working on the displaced electrons via Coulombic attraction.^[73]

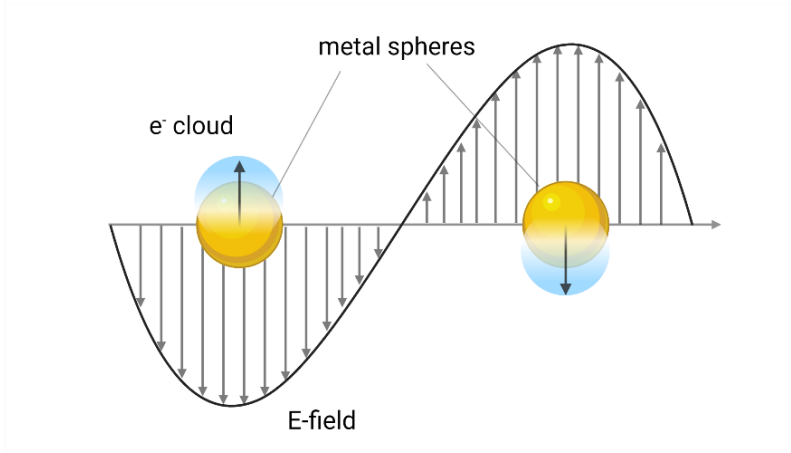


Figure 2.2: Schematic illustration of EM induced electron movements in AuNPs.

Increasing the size of the NP will increase the distance between the positive nuclei and the displaced electrons, weakening the Coulombic attraction and redshifting the resonance peak. Furthermore, the induced fields upon resonance act inside and outside the NP, and if the field lines pass through an external medium with high refractive index (RI), the restorative force is weakened and thus also leads to a redshift

of the resonance peak. The redshift is proportional to the change in RI and can be used for probing the NP surroundings and the adsorption of molecules to the NP (Figure 2.3). In most biosensing applications, the adsorption or binding of a specific molecule is of interest. Either to confirm its presence, quantify the concentration, or study the binding kinetics.^[73]

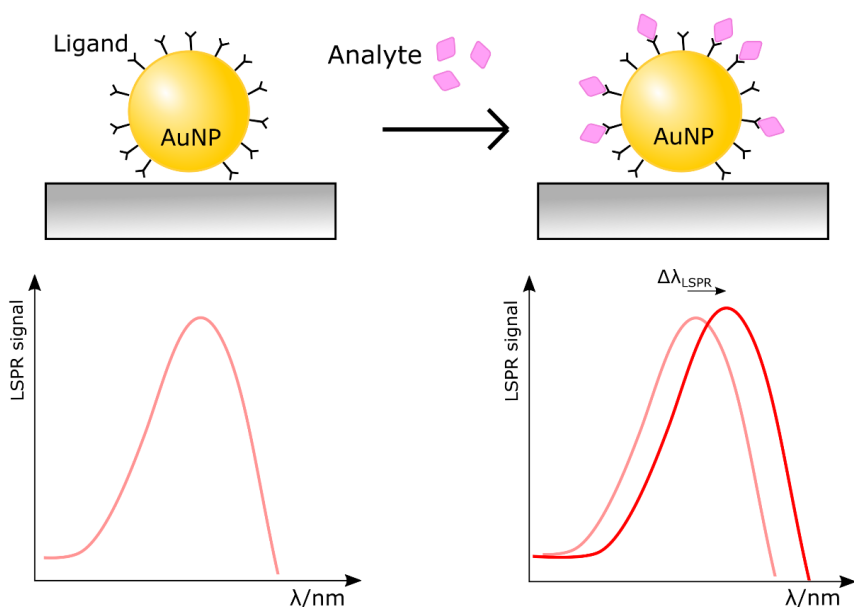


Figure 2.3: Schematic illustration of LSPR based RI sensing indicating the redshift of the LSPR peak as a result of molecular recognition at the nanoparticle surface.

Au is the most commonly used metal for sensing using plasmonic NPs due to the ease of manufacturing of AuNPs and their high chemical stability. AgNPs displays higher RI sensitivity than AuNPs but oxidizes readily which complicates their use.^[73,74] AuNPs

show resonance maxima in the visible spectrum allowing their use in colorimetric assays (Figure 2.4). Well-designed LSPR systems can produce a color change noticeable by the naked eye upon RI changes in the vicinity of the NPs,^[75] however more commonly, NP aggregation is used to produce large color changes, easily detectable by the human vision.^[76] When the distance between two or more NPs is reduced to about one NP diameter or less, their electron clouds start to couple, redshifting the resonance peak.^[77]

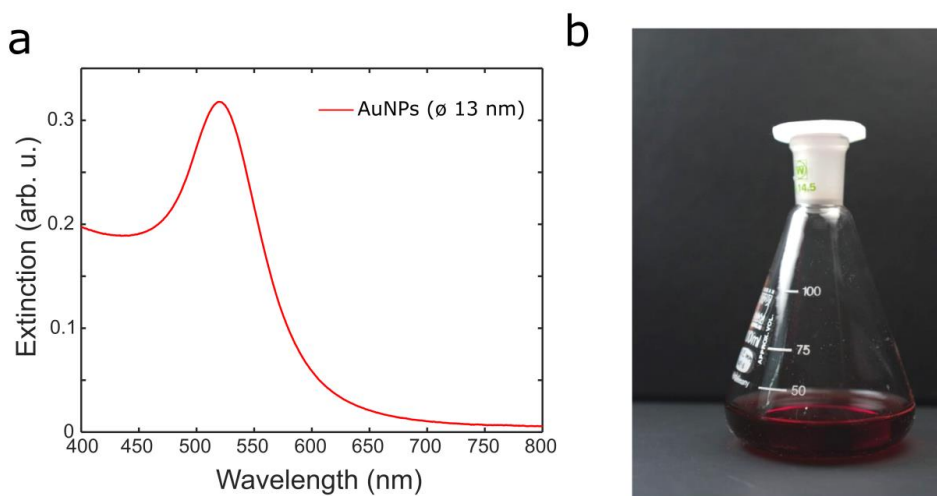


Figure 2.4: a) Extinction spectrum of a diluted AuNP (ø 13 nm) suspension, and b) photo of a red stock AuNP (ø 13 nm) suspension.

There are several processes in which the excited electrons relax,^[72] for example by Joule heating caused by electrons moving through the atomic lattice.^[78] This phenomenon has been utilized for thermal ablation of cancer cells and exploration of new cancer therapies, for plasmon-assisted nanochemistry,^[79] thermoplasmonic nanoelectrodes,^[80] and for solar energy harvesting.^[81]

Nanoparticles for catalysis

Catalysts are employed in a vast number of industrial processes and over 90% of chemicals today are produced using catalysis in one or more steps of the production. They enable such important processes as for example the Haber-Bosch process to create ammonia for fertilizer used in agriculture all over the world.^[82] Some chemical reactions have high energy barriers requiring high temperature and/or pressure for the reaction to occur. Catalysts are compounds that lower the energy barrier for specific chemical reactions simply by being present in the reaction, and without being consumed in the process.

Catalysis can be divided into homogeneous and heterogeneous catalysis where homogeneous catalysis happens with reactants and catalysts being in the same phase, for example by enzymes or metal complexes, in an aqueous solution.^[83,84] Heterogeneous catalysis is conversely where reactants and catalysts are in different phases, such as the conversion of gaseous CO to CO₂ via adsorbing to a catalytic metal surface.^[85,86] The metals used for catalysis are from the groups 8–11 of the periodic table who have favorable electronic composition. These include Fe, Ag, Cu and Pt. Au has previously been excluded from this list due to its highly inert nature,^[87] and it was not until quite recently that the catalytic properties of Au were elucidated. A study by Galvagno *et al.* in 1978 displayed catalytic reduction of NO to N₂ by Au on a solid support.^[88] Catalytic activity of AuNPs on solid supports of different types were further studied by Haruta *et al.* in 1989, showing excellent activity when placed on transition metal oxides, which was hypothesized to be the result of substrate electron transfer.^[85,89,90]

Atomic Au has high reactivity with concurrent high catalytic activity, and as the number of atoms increase, Au clusters are formed which show catalytic activity, especially when constructed by a carefully chosen number of atoms. The difference in catalytic activity between clusters that may be differing in only a few atoms, are due to changes in the bonding and anti-bonding orbitals that heavily influences the ability to adsorb different chemical species.^[85] For heterogeneous catalysis to occur, at least one

reactant must adsorb at the solid-liquid interface. The miniaturization of Au changes the surface structure and increases the number of ridges, facets and surface defects that are present in the system. These places are hotspots for low coordination atoms with unsatisfied orbitals, which allows adsorption to NP through previously mentioned bonding orbitals. The bonding orbitals associated with the metal surface interacts with the adsorbent and weakens its molecular chemical bond, in turn lowering the energy barrier for a chemical reaction to occur.^[85]

However, the harsh synthesis conditions of metal-oxide supported AuNP catalysts limits control over AuNP geometry and requires low sustainability materials such as Co, Ni, Fe, Ce, etc.^[90,91] Exchanging metal-oxides for soft supports allows the use of more sustainable materials, and facilitates recovery of the catalyst for reuse.^[92] In an article by Kuroda *et al.*, poly(methyl methacrylate) (PMMA) was used as a soft substrate after synthesizing AuNPs *in situ* through reduction of gold salt by sodium borohydride (NaBH_4), a commonly used reducing agent for synthesis of AuNPs.^[21] The resulting materials was then used for catalyzing the reduction of 4-nitrophenol (4NP) to 4-aminophenol by NaBH_4 . This reaction has become a model reaction for probing the catalytic efficiency of different catalysts and was used in **Paper IV** to study the catalytic performance of BC-NP composites.^[93]

Substrates for nanoparticle immobilization

Two-dimensional substrates

As discussed in chapter 2, adsorbing NPs on a solid substrate can simplify the handling of the NPs and can enable new applications. If the interactions between the NPs and the substrate are sufficiently strong, the issues relating to colloidal stability typically encountered with NPs in suspension can largely be ignored. For catalysis, for example, the NPs can be used in applications where the conditions, including reactants, products, or solvents, that would otherwise interfere with colloidal stability. In addition, when immobilized on a substrate, the retrieval of NPs from a reaction vessel is facilitated, allowing the reuse of the catalysts. Similarly, the potential applications of plasmonic metal NPs are expanded when immobilized on solid supports. The use of plasmonic NPs in RI biosensing has garnered much attention in the last decades. Specific analyte recognition requires the functionalization of NPs with ligands as well as molecules that can prevent unspecific binding of other compounds to the NP

surface. However, both the surface chemistry, analyte binding, and sample matrices can have large and often negative effects on the colloidal stability. The immobilization of NPs on solid supports circumvents these issues which substantially simplifies their use in several applications,^[69,94,95] and enables their use in for example real-time monitoring of biomolecular interactions.^[96]

Two-dimensional (2D) (i.e. flat) substrates, such as glass, silicon, or polypropylene, have been widely used for immobilization of plasmonic NPs for biosensor applications.^[68,71,97–102] Numerous techniques and surface chemistries have been developed to control and optimize the NP immobilization process on such substrates.^[103]

However, in addition to being mechanically stiff and thus not suitable for e.g., wearable biosensors, the maximum surface density of NPs is highly limited on 2D substrates. Too high NP surface density results in optical coupling between the NPs and a broadening of the LSPR band, which decreases the figure of merit (FOM) value and thus the sensor performance. The number of particles that can be immobilized on a substrate before NP coupling occurs depend on the total available surface area of the substrate, which is typically low for flat substrates. The low NP number can be especially problematic for RI biosensors, where the signal-to-noise ratio improves with increasing NP surface density. The use of soft three-dimensional (3D) substrates allows for immobilization of larger number of NPs on mechanically flexible materials, which opens up for development of new sensor concepts and applications. Moreover, the possibilities to use flexible 3D substrates that can incorporate large number of NPs while maintaining a surface density that does not cause NP coupling, can enable design of materials with previously unknown properties.

Bacterial cellulose

Biopolymers are polymeric materials of natural origin. Examples of biopolymers include alginate^[104], chitin and chitosan,^[105,106] and cellulose, which have been used and explored in a wide range of biomedical applications, such as 3D cell culture,^[107] tissue engineering,^[108] drug delivery,^[109] and as advanced wound dressings.^[107]

Cellulose is the most abundant biopolymer on earth and is a fundamental part of plant cells, residing in the cell wall, providing structural strength to the cell. Cellulose has been used throughout human history as a source of heat, building material, and for clothing. Wood pulp is the most common source of cellulose and is used in a variety of products such as paper and cardboard, textile for Lyocell, as additive in pharmaceuticals, foods, and cosmetics.^[110,111]

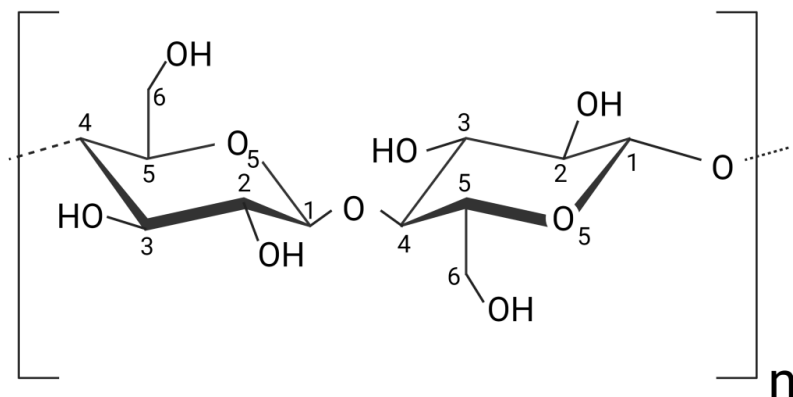


Figure 3.1: Schematic illustration of the molecular structure of one cellulose repeat unit.

Cellulose is a carbohydrate and consists of repeating units of D-glucose, covalently linked into long chains through a glycosidic bond between the C4 and the C1 carbon (Figure 3.1). Cellulose polymers in wood pulp can comprise a couple of hundred up to slightly above one thousand glucose units while cellulose from other plant fiber chains can have as many as 10 000 monomers.^[110]

There is substantial evidence for intra-molecular hydrogen bonding between hydroxyl groups at C3 and O5 leading to a flat cellulose chain conformation. Furthermore, it is likely that hydroxyl groups at C2 and C6 also form intra-molecular hydrogen bonds that add to the high axial stiffness of the cellulose chain. Moreover, these hydroxyl groups seemingly interact with neighboring cellulose in-plane (side by side), whereas

the level of hydrogen bonding between stacked chains is more uncertain. Instead, cellulose chain stacking interactions seem to be dominated by van der Waals-forces, which could explain the difficulty of dissolving cellulose in water, despite the hydrophilic nature of the cellulose chain.^[110,112–114] Slight differences between cellulose chain packing lead to several types of crystalline cellulose. Type I cellulose is the type found in nature and can be converted to other crystal structures through chemical and mechanical processes. These other crystal structures, II, III and IV display varying kinds of stability with type II showing greatest stability of the technically relevant crystal structures.^[110,111]

Larger cellulose structures such as fibers, fibrils and sheets contain crystalline and amorphous regions to a varying degree depending on cellulose source and processing. The amorphous regions constitute disorganized cellulose chains and give the structure its flexibility due to weaker interchain bonding. These amorphous regions are more easily permeated by additives and chemicals and the degree of crystallinity therefore influences the ease with which it is possible to chemically hydrolyze the cellulose structure or modify the cellulose molecules. Acid hydrolyzation is utilized to remove amorphous sections and create cellulose nanocrystals (CNC) with high cellulose content, high crystallinity, and high aspect ratio (3–70 nm in width and 25–3000 nm in length) that have been frequently used in combination with different polymers for making nanocomposites.^[115]

CNC in water, together with BC, show birefringent properties as a result of the anisotropic structure of cellulose at most length scales.^[110,115] In the last decades, BC films with very high transparency have been reported by Nogi *et al.*^[116] for use in high-performance optical applications. However, cellulose-based materials such as paper consist of larger subunits (thick fibers or fibrils), which results in extensive scattering of light in the visible wavelength region, giving them a white appearance.

As previously mentioned however, there are non-plant sources of cellulose. Bacterial cellulose is produced by several different species of bacteria, for example *Komagataeibacter xylinus*, which under aerobic conditions converts different types of

simple carbohydrates to cellulose. BC's function for bacteria is hypothesized to be similar to other types of extracellular polymeric substances (bacterial biofilms), that is to protect the bacteria from external threats like desiccation and predators, and to form pockets of nutrients which facilitates growth.^[111,117]

Unprocessed pieces of BC appear translucent if pellet thickness is low (Figure 3.2), but can be opaque with increasing pellet thickness. As with plant cellulose, this phenomenon is due to light scattering which is a result of nanoparticle/fibril size and RI contrast between solvent/medium and BC fibrils, and can be reduced if immersed in a material of similar RI as shown by Yano *et al.*,^[118] They successfully produced a BC nanofibril/epoxy resin composite with the excellent light transmittance properties of epoxy resin and enhanced mechanical stability in comparison to neat resin, due to the incorporation of BC nanofibrils. This has made BC an interesting material for providing composites for optical applications.^[119]

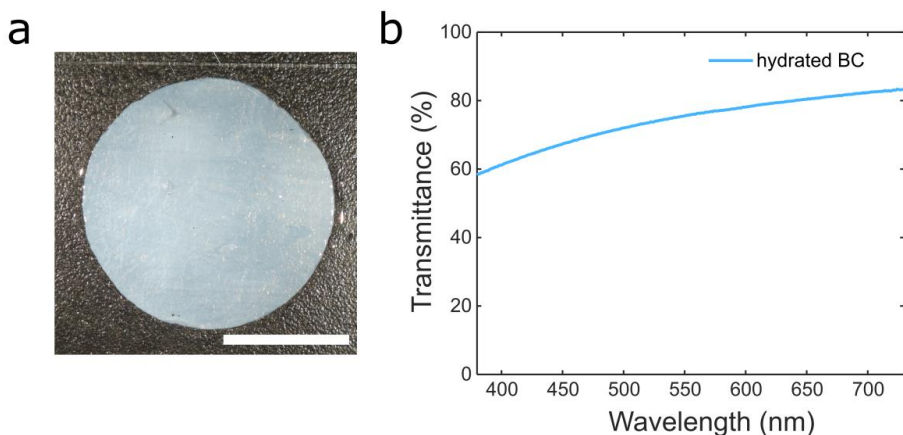


Figure 3.2: a) Photo of hydrated BC (scale bar: 1 cm). b) Transmittance spectrum of hydrated BC.

To purify plant cellulose, several processes are undertaken in order to remove hemicellulose and lignin. Lignin and hemicellulose are tightly connected to the cellulose and are thus very difficult to remove. Bacteria do not produce hemicellulose

or lignin and BC is therefore very pure, requiring only washing in alkali solutions to remove bacteria and metabolites that may be present.^[120,121] Without additional processing, BC has a high degree of crystal structure (type I) with fibril diameters of 70-100 nm and roughly a micron in length. Due to the high degree of crystallinity, chemical modifications of BC happen mostly at the fibril surface. Several different types of strategies have been developed to tune the functionality of BC through modifications of surface chemistry, such as acetylation,^[122] sulfonation,^[123] and TEMPO-oxidation.^[124,125] TEMPO-oxidation results in carboxylic groups on the BC fibril surface which can be further functionalized using e.g., carbodiimide chemistry (EDC/NHS). Other surface functionalization protocols also exist where compounds have been physisorbed to the surface of the fibrils or trapped in the fibrillar network. One example that has been trapped in BC is silver sulfadiazine,^[126,127] a drug for treatment of infections in burn wounds. Silver has bactericidal effects, presumably through the interactions between silver ions and for example, the microbial DNA, the cell membrane and other vital cellular structures, and has been widely used in different formulations to treat wound infections.^[128] Furthermore, AgNPs have through different means been *in situ*-synthesized on BC fibrils to form antimicrobial BC-AgNP composites for advanced wound care.^[129–131]

Bacterial cellulose as a wound dressing material

BC has several useful qualities for development of wound dressings. BC is a hydrogel and retains moisture very well, which is beneficial for wound healing. The hydrogel is highly flexible which makes it suitable for placement on joints and flexing body parts. Additionally, the flexibility allows the BC wound dressing to conform well to tissues, efficiently covering the wound bed and reducing pain through close contact with exposed nerve endings.^[132] The high degree of natural cross-linking makes the hydrated fibrillar network in BC durable, which facilitates handling of the dressings. The nanoporous, fibrillar BC network is also permeable to gases, while preventing bacteria from entering the wound. Furthermore, BC shows exceptionally low toxicity to human cells and clinical studies on BC have shown good results. In a study by Santi *et al.*, burn wounds were covered with BC and showed excellent healing for all five

participants after less than 40 days.^[133] Diabetic leg ulcers, which are notoriously difficult to heal, often lasting months or years without healing and causing immense suffering for the patient,^[134,135] have also been successfully healed when treated with BC wound dressings.^[136] In a study by Sivilér *et al.*, where BC dressings were evaluated for treatment of chronic ulcers, most patients did not require a single dressing change until the wound had healed. In comparison, other advanced wound dressing materials would typically require one or two dressing changes per week.^[137] Changing a wound dressing damages the wound bed and retards or disrupts healing. BC wound dressings simply incorporate into the produced scab and falls or peels off after the wound is completely healed.

The usefulness of BC as a wound dressing material has spurred interest in functionalization of BC to achieve functional wound dressing materials for advanced wound care. For instance, treating wound infections by incorporation of silver containing compounds, e.g. AgNPs, as previously mentioned.^[126,127] Additional routes for resolving wound infections have been investigated, for example by immersing dried BC in antibiotics or other antimicrobial compounds that will be released in the wound to reduce occurrence or severity of infections.^[138] In addition, sensors for detection of infections have also been developed using BC as a scaffold for the sensor transduction mechanism. Integrating the sensor in the wound dressing reduces the need to remove the dressing to assess wound status, and also enables close contact between the sensor and the wound tissue.^[139]

Wound pH is an indicator of healing progression and can become elevated during infections and chronification of wounds.^[140,141] For this reason, pH sensors featuring different pH-responsive modalities that can give information on wound pH without the use of elaborate measuring technologies can allow patients or healthcare personnel to detect early signs of infection. Such sensors are often based on colorimetry and have been combined with a number of different wound dressing materials.^[142–145] Possibilities to monitor wound pH may significantly improve the outcome of wound infections since the pH changes commonly manifest before clinical symptoms have appeared, giving a chance to diagnose and treat the infection at an early stage, reducing risk of complications such as sepsis. There are however other types of sensors that can help diagnose wound infections based on sophisticated sensor designs. For instance, colorimetric,^[146] potentiometric and fluorometric pH sensors.^[147,148] The fluorometric

sensor by Jankowska et al. was also able to measure glucose levels in the wound. Furthermore, temperature sensors based on electrical and optical transduction mechanisms have also been developed, with potential use for advanced wound care.^[149,150]

In addition, nanoplasmonic based sensors have also been studied for advanced wound care. Belushkin *et al.*, devised a procalcitonin and c-reactive protein sensor for diagnosing sepsis through the use of an plasmonic microarray enhanced with AuNPs.^[29] As mentioned in the previous chapter, AuNPs have been used for refractometric sensing for a few decades and has recently been combined with a number of different biopolymers, including BC, for different sensing applications.

Wound healing is a complex process involving formation of new tissue and remodeling of already existing tissue. Proteases are a class of proteins that are heavily involved in tissue remodeling due to their enzymatic activity towards proteins and peptides. Excessive proteolytic activity may disrupt the normal healing process and delay wound healing, potentially leading to the chronification of wounds.^[151] Bacteria excrete proteases to break down surrounding tissue in order to access nutrients needed for their growth and proliferation. In addition, some bacteria can activate enzymes endogenous to the human host, matrix metalloproteinases (MMPs), which further increases proteolytic activity.^[152] Bacterial infections in wounds therefore increase the total proteolytic activity which can be used as a biomarker for bacterial infections, a concept that has been used for development of lateral flow devices and microfluidic chips for infected wound fluid.^[153,154] Developing a sensor for proteolytic activity was also the aim of **Paper III**.

Synthesis and application of BC-nanoparticle composites

State of the art

Similar to the incorporation of AgNPs in BC for their antimicrobial effect, AuNPs have been immobilized in BC using comparable techniques, i.e., by direct reduction of gold salt in the presence of BC fibrils. BC combined with plasmonic NPs have gathered a lot of attention due to the multitude of applications of such NPs when combined with the interesting material properties of BC as a three-dimensional substrate. For example, BC functionalized with plasmonic NPs can be utilized for development of sensors, facilitated by the relatively good transparency of thin BC sheets to light in the visible wavelength range. AuNPs are more frequently used in plasmonic sensors than AgNPs due to their better chemical stability.

AuNPs have been synthesized in BC from HAuCl_4 without any additional reduction agents as described by Morales-Narvaez *et al.*^[155] Here, the reduction by BC alone (and

potentially other organic species remaining from the BC production) was sufficient to form AuNPs in less than 2 hours at boiling temperature. The resulting composite material was explored in an aggregation assay for detection of thiourea and cyanide by monitoring the spectral changes of the NPs. Similarly, Pinto *et al.*, successfully performed reduction of H₂AuCl₄ using only BC as a reducing agent, although they also investigated a sodium citrate route which likewise resulted in BC-AuNP composites.^[156]

Another strategy to produce BC-AuNP composites was described by Chen *et al.*, where AuNPs were synthesized directly in BC using surface modified BC.^[93] The BC fibrils were functionalized with amidoxime groups that sequestered the Au ions, resulting in AuNPs of roughly 13 - 16 nm diameter for use in catalysis.

BC surface modifications using non-covalent interactions, such as electrostatic adsorption of the polyelectrolytes polyethyleneimine (PEI), and poly(diallyldimethylammonium chloride) (PDDA) in a layer-by-layer (LbL) fashion was used by Pinto *et al.*^[156] NP adsorption via LbL uses oppositely charged polyelectrolytes applied consecutively to precisely control layer thickness and to achieve positive surface charge, and has been utilized to achieve homogeneous adsorption of citrate stabilized AuNPs to e.g. 2D glass substrates since the late 90's.^[74,96,98,157] Pinto *et al.*, used the technique on a 3D substrate.

PEI adsorbed to BC fibrils can also be used as a reduction agent, leading to the formation of relatively monodispersed AuNPs in high concentrations as demonstrated by Zhang *et al.*^[158] Interestingly, they showed that synthesis of AuNPs in different solutions containing halide salts of different types, NaF, NaCl, NaBr and NaI, heavily affected the number of AuNPs at the BC fibrils. They subsequently discussed how the affinity between BC and Au could be higher for heavier members of the halide group and that the heavier halide ions diminished the repulsive interactions between particles or Au⁺ ions and BC by electrostatic screening, which allowed for smaller interparticle distances between Au species BC fibril surface.

None of the *in situ* synthesis methods provide AuNPs with sufficiently high uniformity for use in refractometric sensing. As discussed in chapter 2, refractometric sensing measures small shifts in the position of the LSPR peak caused by changes in RI close

to, or at the NP surface. RI changes happen when for example an analyte binds to a ligand at the NP surface or due to physicochemical changes, such as buffer content, ionic strength, or changes in temperature. To facilitate the quantification of the peak shift, a sharp LSPR peak and a large signal-to-noise ratio (S/N) is of high importance. Sharp peaks are a feature of monodisperse, small NPs with little to no plasmonic coupling, whereas large S/N is a result of good instrumentation and a high number of particles. Furthermore, the lack of control of interparticle distance between immobilized AuNPs often leads to plasmonic coupling and subsequent broadening of the resonance peak.

The hitherto known examples of colloidal NPs immobilized in BC through means of self-assembly are found in two articles from 2016 by Tian *et al.*, who achieved loading of a high number of gold nanorods (AuNRs) through electrostatic interactions between positively charged surfactants, CTAB, on the AuNRs and the negatively charged BC surface.^[59,159] While their resulting biofoam appeared opaque due to the large number of immobilized AuNRs, UV-vis measurements showed little plasmonic coupling between NPs and retained peak sharpness from colloidal AuNRs. CTAB, and similar surfactants are highly cytotoxic and are thus not well-suited for applications in biological systems.^[160,161] While washing may alleviate most of the toxicity for AuNRs,^[162,163] spherical AuNPs with CTAB still exhibit some cytotoxicity.^[164] Overall, citrate stabilized NPs have a more favorable toxicity profile and are preferable in several applications. Additionally, CTAB interaction with NPs is very strong, which complicates further functionalization and modification of the NP surface.

Self-assembly of citrate stabilized AuNPs to BC

As previously mentioned, the self-assembly of citrate stabilized AuNPs to BC is more complex than CTAB stabilized NPs since both citrate stabilized AuNPs and BC are negatively charged. Citrate stabilized AuNPs can, however, adsorb to BC fibrils under special conditions as shown in **Paper I**. The assembly process is hypothesized to be due to attractive van der Waals interactions between the NP and the BC fibril. All surfaces can interact via van der Waals forces, which are very short-range forces, decaying with $1/r^6$ and therefore requires short distances between the NP and the fibril

surface to bind with sufficient strength. However, for NPs to get close enough for van der Waals forces of any significance to arise, the repulsive interaction between the electric double layers at the respective interfaces must be overcome. We modelled the interaction between a particle and a negative BC halfspace (Figure 4.1a), showing that the potential barrier ($V/k_B T$) arising from the surfaces respective electric double layer decreases as the buffer ionic strength increases (Figure 4.1b). At some ionic strength, here modified using a monovalent halide salt, NaCl, the potential $V/k_B T$ becomes negative and the self-assembly is spontaneous at RT (Figure 4.1c).

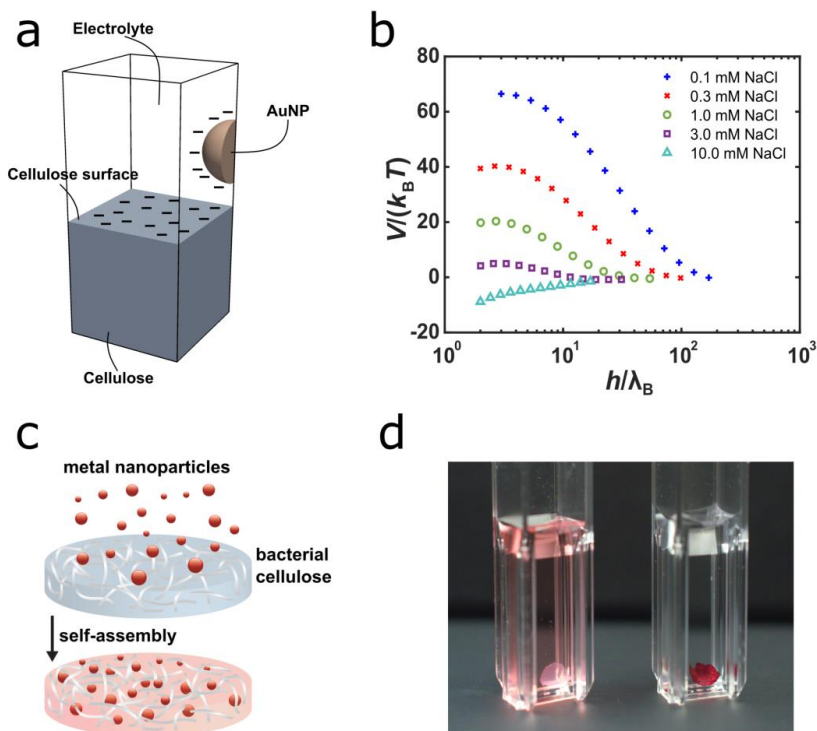


Figure 4.1: Self-assembly of AuNPs to BC. a) Gold sphere interacting with a flat cellulose halfspace in an electrolyte (monovalent). b) Simulated potential of interaction as a function of distance between gold sphere and cellulose. c) Schematic of self-assembly of NPs to BC. d) BC incubation in aqueous AuNP (ϕ 50 nm) suspension before (left) and after complete depletion of suspended AuNPs (right).

However, decreasing the $V/k_B T$, by increasing the ionic strength, simultaneously decreases the potential barrier between NPs, risking irreversible NP aggregation. It was found that using 10 mM NaCl buffer did not work for citrate stabilized AuNPs of -66 mV ζ -potential due to extensive NP aggregation, however 5 mM NaCl was sufficient to achieve high adsorption of AuNPs to BC (ζ -potential \approx -46 mV) (Figure 4.1d).

The absorbance of the resulting BC-AuNP, which is correlated to the number of particles in the measuring path, was increased 6-fold when compared to a 2D substrate (Figure 4.2a), enabled by the 3D fibrous structure of BC, while leaving the FWHM unchanged (Figure 4.2b).

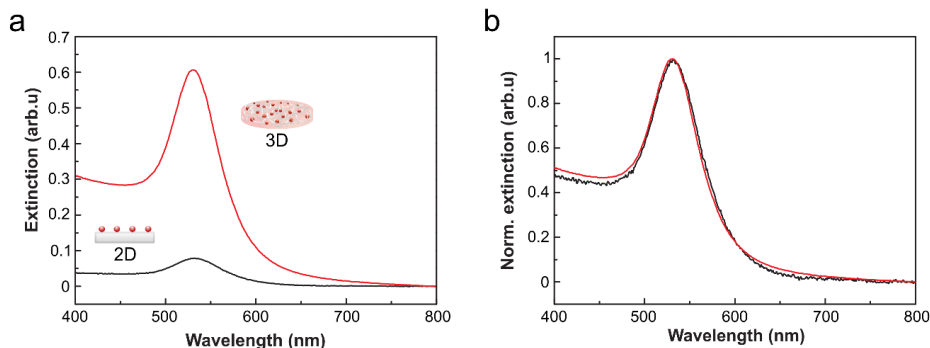


Figure 4.2: Optical properties of BC-AuNP (ø 50 nm). a) Extinction spectra of BC-AuNP (3D) and glass (2D). b) Normalized extinction spectra of BC-AuNP and glass.

Refractometric sensing often relies on detection of very small (<10 nm) LSPR peak shifts. The large increase in signal strength concurrently increases the signal-to-noise ratio (S/N). Reducing noise is a good way to achieve a high S/N, however reducing noise beyond a point becomes tedious, expensive, and even impossible. Boosting the signal strength is therefore a good way to improve S/N and thereby sensor performance. [73] Analysis techniques like polynomial fitting are useful to find the correct peak position from discrete data points. The accuracy with which the peak can be determined is highly impacted by the S/N which can be understood from comparing the data quality of the peak for different S/N systems (Figure 4.3). In **Paper I** we show that BC-AuNP composites were able to discriminate between peak shifts a factor 2.3 times smaller than using the conventional glass substrates.

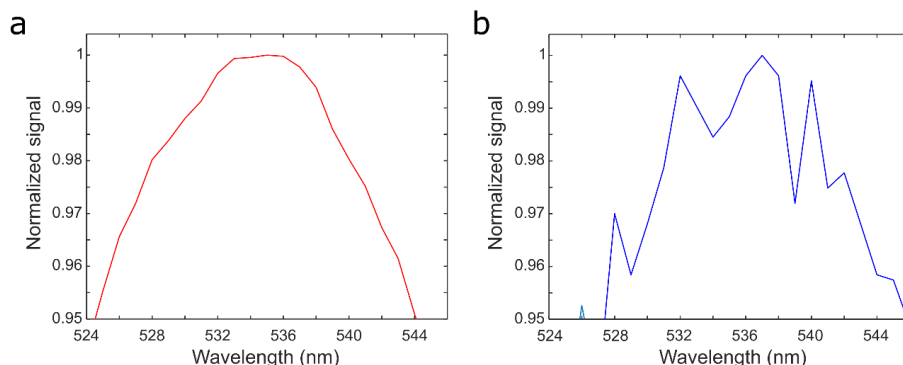


Figure 4.3: Zoom in of the LSPR band for a high (a) and low (b) S/N system.

Mechano- and thermoplasmonic properties

The hydrated 3D BC matrix consists of well-separated fibrils and is soft and pliable. The AuNPs present in BC after adsorption of a moderate amount are well-dispersed on fibrils throughout the BC matrix. If sufficient pressure is applied to BC, water is evacuated from the structure and the distance between fibrils is decreased. If NPs are present on the fibrils, the distance between these will also decrease. As mentioned in chapter 2, when the particles are brought in close proximity, near-field interactions cause spectral changes dependent on interparticle distance (Figure 4.4a).^[77,165–167] The spectral changes due to BC-AuNP compression could be seen as a redshift of the LSPR maximum concurrent with a pronounced broadening of the LSPR maxima presented as a shoulder at around 600 nm (Figure 4.4b). Near-field interactions increased with increasing pressure and was shown to be irreversible. However, the slight redshift was mostly reversed upon relieving pressure. Interestingly, adsorbing a protein, bovine serum albumin (BSA), to the BC-AuNP by immersing the composite in a high concentration solution of 10 mg/mL for 2 hours almost completely inhibited the occurrence of near-field interactions for the same level of compression. The redshift of the LSPR maximum was obtained also in this case but was similarly reversed upon reducing pressure. The capability of BSA to prevent near-field interactions formed a rudimentary biosensor where adsorbed species can modulate the changes in optical properties upon compression. The biosensor was subsequently tried for different

concentrations of BSA and was able to distinguish between 10 and 100 nM BSA (**Paper I**).

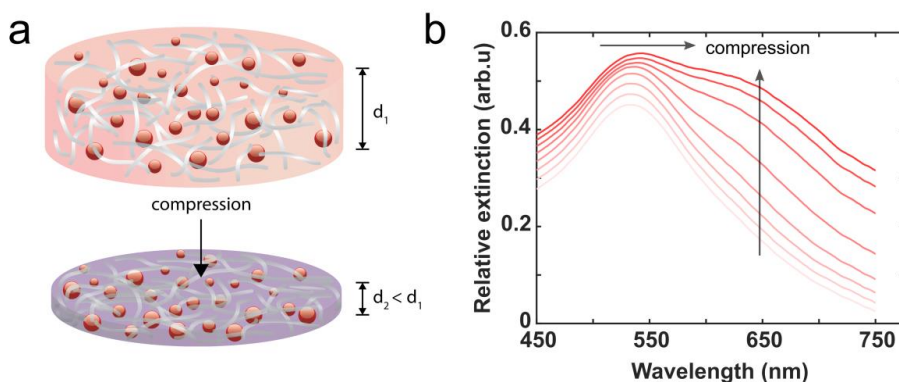


Figure 4.4: a) Schematic illustration of the mechanoplasmonic behavior in BC-AuNP and the resulting color shift upon compression. b) Spectral changes in BC-AuNP due to compression.

The compression of BC-AuNPs and the resulting change in optical properties affected the absorbance cross section of the composite (Figure 4.5a). The AuNP aggregates formed when AuNPs are brought in close proximity upon compression of the BC-AuNP composite effectively act as a larger NP. As evident from equation 2.1, absorption cross section is dependent on the size of the NPs. Higher cross sections lead to higher light-heat conversion upon illumination.^[78,79] This made it possible to modulate the thermoplasmonic properties of BC-AuNP through compression (Figure 4.5b)

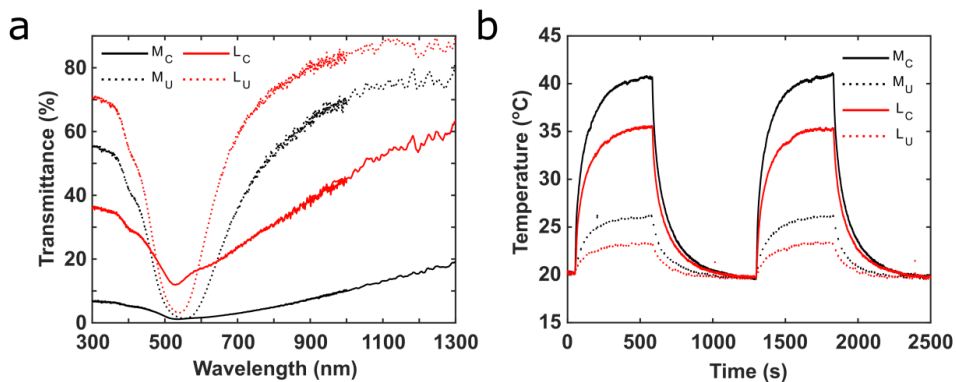


Figure 4.5: a) Transmittance of BC-AuNP loaded with two different concentrations of AuNPs prior to and after compression. b) Heat generation due to plasmonic heating when irradiated with two laser diodes (808 and 1064 nm). “M”, and “L” indicate medium and low AuNP concentration respectively, while subscript “u” and “c” corresponds to uncompressed and compressed, respectively.

Broadband adsorbing properties of self-assembled BC-AuNP composites

Evidently, the change in surface potential upon adsorption of AuNPs is not large enough to prevent subsequent NP adsorption. Highly concentrated AuNP suspensions will, given sufficient time, form BC-AuNP composites with huge amounts of particles, where interparticle distance is very low or zero, forming AuNP aggregates on the BC surface. Likely, adsorbed NPs retain a higher ζ -potential than the surrounding BC, leading to repulsive forces strong enough to space AuNPs somewhat homogeneously over the surface before starting to aggregate.

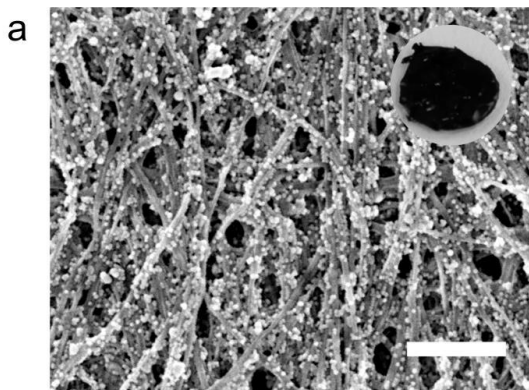


Figure 4.6: a) SEM micrograph and photo (inset) of BC-AuNP incubated in a high concentration AuNP suspension. Scale bar: 500 nm.

The large amounts of NPs and NP aggregates (Figure 4.6a) lead to a very high extinction in the visible spectrum, resulting in a profoundly black appearance (Figure 4.6a inset), in part due to the composite surface structure. Material surface structure is very important for the absorptive properties of a material as shown by McCoy *et al.*^[168] They showed how structure in some bird species feathers allows much deeper black colors than feathers achieving black features by molecular absorption (pigments) alone. The black appearance was retained even after the feathers were coated in a highly reflective metal coating.^[168] Ridges and other surface structures are hypothesized to be able to trap electromagnetic radiation of different wavelengths depending on the length scale of the existing surface roughness. This was further shown by Tao *et al.*, who converted a highly reflective Al surface to highly absorptive by introducing surface roughness via laser filament processing.^[169] The grooves and pillars exhibited plasmonic behavior which led to a large absorption cross section. Together with iterative reflections inside the structure, the high absorption cross section only allowed for a few photons from the incident light to escape, resulting in a very black appearance. Plasmonic AuNPs and other Au-based structures have been used for creating broadband, ultra-black materials.^[170,171] For instance in black Au-based films for solar-harvesting applications.^[81] The 3D structure of BC may similarly affect the absorptive properties of BC-AuNP which we studied in **Paper V**. Like many of the ultra-black materials, one of the main reasons for the highly absorptive properties of hydrated BC-AuNP is the limited reflection from the material.^[168,170,172,173]

Substrates with a sharp change in RI will have higher reflectance than lower RI substrates in the same medium. In accordance with this reasoning, we found that air-drying BC-AuNP, a process which compacts the BC structure, resulted in higher reflectance than freeze-drying, which to a higher degree conserves the fluffy, porous structure of hydrated BC-AuNP. The low density of freeze-dried BC-AuNP likely leads to a more diffuse RI transition and thus a lower reflectance. The hydrated BC has the same low-density structure as freeze-dried BC-AuNP with the added layer of water ($n \approx 1.3330$) between air ($n \approx 1$) and cellulose ($n \approx 1.49$ at 700 nm) and NP interfaces, adding to the stepwise decrease and further lowering the reflectance.^[174,175]

Catalytic properties of self-assembled BC-NP composites

Using substrates for catalysts is beneficial for reasons previously discussed, such as catalyst recyclability and a possibility to disregard NP colloidal stability. Since the AuNPs are the catalytically active components it is preferable to maximize the number of AuNPs per volume or weight unit substrate. In **Paper IV**, we studied the effect of loading large numbers of AuNPs, PtNPs and AgNPs to BC on catalytic rate of a model reaction, namely the reduction of 4NP to 4-aminophenol by NaBH_4 . BC-PtNP showed higher catalytic rate than AuNPs and AgNPs which is not surprising for NPs of roughly 10–13 nm. Although the structure of BC is highly porous, diffusion is slow in comparison to the catalytic rate, which meant that diffusion is limiting the reaction speed. Additionally, the H_2 gas that was released during the reaction formed gas bubbles that was trapped in pockets in the fibrillar mesh, blocking the flow of reagents through the BC structure. To avoid this, BC was processed with ultrasonication to disrupt the membrane integrity. The imploding cavitations caused by the ultrasound waves carries enough energy to cut amorphous regions in the BC fibrils, dissociating and shortening the fibrils. Since BC has a high crystallinity, and the crystalline regions are largely stable enough to withstand mild sonication procedures, the sonication process leaves a fuzzy, disentangled structure mostly consisting of crystalline BC fibrils.^[176,177] Dissociation of pre-formed BC-AuNP composites via ultrasonication could be successfully achieved with NPs still attached to BC fibrils. However, ultrasonication of BC before mixing with AuNP suspension resulted in almost

instantaneous adsorption of AuNPs to BC (D.BC-AuNP). The very fast adsorption is likely due to removing the mass transport limitations by having individual suspended fibrils. Additionally, ultrasonication may affect the ζ -potential of BC fibrils to allow more favorable NP-fibril interaction.^[64] Both the dissociated pre-formed BC-AuNP (dis. BC-AuNP) and D.BC-AuNP displayed similar catalytic properties as BC-AuNP composites but showed a much higher catalytic rate as compared to intact BC membranes (Figure 4.7), in line with the improvements in mass transfer of reactants to the NP surface.

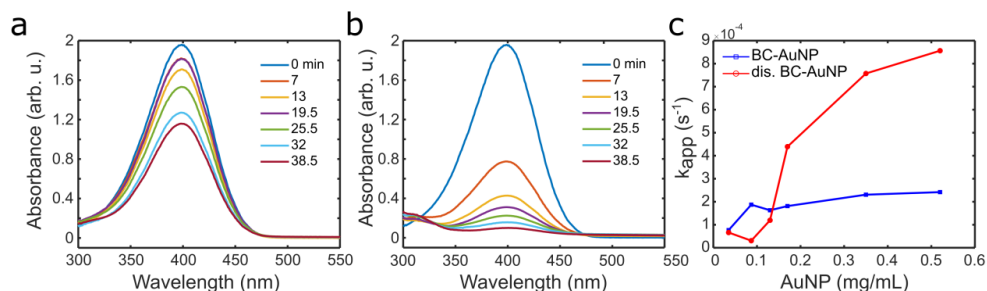


Figure 4.7: Time-resolved UV-vis spectra of 0.5 mg/mL a) BC-AuNP and b) dissociated BC-AuNP. c) Catalytic activity vs AuNP content for BC-AuNP and dissociated BC-AuNP.

BC-NP composites for advanced wound care

Paper II and III drew inspiration from BC's excellent wound dressing material characteristics and combined BC with NPs for added functionality for advanced wound care. In **Paper II** BC was incubated in a suspension of MSNs, ~400 nm in width with ~10 nm diameter pores. Like the citrate stabilized NPs, MSNs also showed adsorption to BC fibrils, despite their size (Figure 4.8). The MSNs probably interact with several fibrils at once to bind sufficiently strong not to desorb. As seen from the SEM micrographs in Figure 4.8, BC-MSN are aggregated or clustered in the BC matrix. It is not unlikely that the MSNs are in a semi-aggregated state already in the loading suspension, although they may also aggregate on the BC surface similar to citrate stabilized AuNPs, given enough time. Increased aggregation due to the drying process in preparation for imaging is also possible. In contrast to colloidal AuNPs, MSNs are in a dry state before resuspension, and ultrasonication is used to disperse and

resuspend the MSN aggregates prior to use. As such, it is possible that the ultrasonication procedure is insufficient to produce individual MSNs, and that the loading suspension is comprised of MSN aggregates of different sizes.

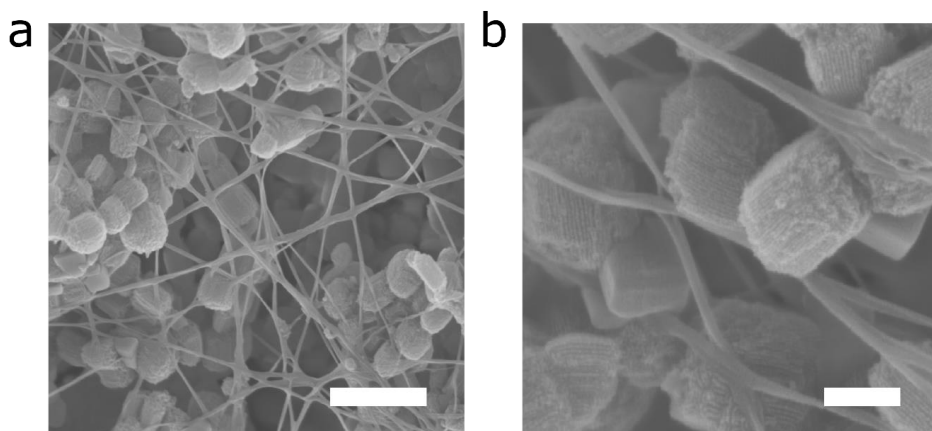


Figure 4.8: SEM micrographs of BC-MSN, showing aggregated and individual MSN attached to BC fibrils. Scale bar: a) 1 μm , b) 200 nm.

As previously mentioned, MSNs have pores which gives them a large specific surface area that make them suitable carriers for molecules for added functionality or drugs in drug-delivery applications. Here, we were interested in detecting the pH of a wound and thus encapsulated a pH-responsive dye, bromothymol blue (BTB). BTB retained its pH-responsiveness after being adsorbed in the BC-MSN composite (Figure 4.9a,b,c). By following the relative peak intensities of BTB functionalized BC-MSN it was possible to distinguish between different pH values optically (Figure 4.9d).

Upon infection, the wound pH commonly increases and becomes alkaline,^[140,141] where BTB displays a deep blue color. Blue is among the few colors usually not present in wound tissue, neither in infected nor healthy wounds. MSN-BTB functionalized wound dressings will consequently show good contrast to the wound at alkaline pH values, giving a clear indication of infection to healthcare professionals without the need for complex instrumentation for sensor readout.

The mechanical properties of the dressing were largely intact and even enhanced upon MSN functionalization, since the MSN decreased the stress relaxation rate which makes the BC-MSN more resistant to moderate pressure levels (~12 kPa). They may hence perform better when applied at e.g., joints compared to native BC. Moreover, the change in pH was reversible and fast (< 10 minutes) and could therefore potentially be used for studying the effect of treatments on wound infection in a spatiotemporal fashion.

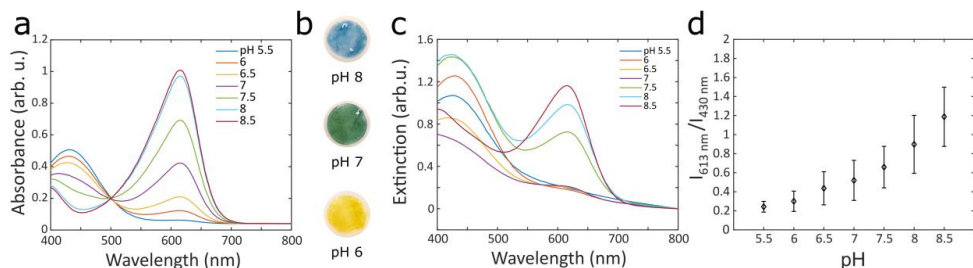


Figure 4.9: a) UV-vis spectra of BTB in buffers with different pH values. b) Photo of BC-MSN functionalized with BTB after immersion in buffers with different pH. c) UV-vis spectra of BTB functionalized BC-MSN composites. d) Relative peak intensity of BC-MSN composites in (c).

In **Paper III** we also aimed to detect wound infections but used protease activity instead of pH as an indicator for bacterial infection. Plasmonic NPs have been used to probe the activity of bacterial proteases refractometrically as described by Svård *et al.*^[178] Proteolytic activity has been identified as a biomarker for wound infections as discussed in chapter 3. We designed a BC-AuNP composite functionalized with a fluorescent dye, Cy3, conjugated to protease substrates (casein) adsorbed to the AuNP surface. The positioning of Cy3 in the vicinity of AuNP quenched the fluorescent signal and resulted in a very low fluorescent signal. The little fluorescence that could be measured was likely due to Cy3 conjugated to casein that was not bound to an AuNP but adsorbed directly to a BC fibril. When adding a model protease, trypsin, the casein-Cy3 was cleaved to smaller fragments, free to diffuse away from the AuNP. Since AuNP-Cy3 quenching is heavily distance dependent, diffusing just a short distance from the AuNP led to a fluorescence recovery that could be measured in a microplate reader. To acquire higher specificity towards wound relevant proteases, we synthesized a short

peptide, CPI2, with a thiol containing amino acid, cysteine, in one end, and a Cy3 dye in the other end. The thiol group can bind covalently to gold, adding specificity also in the functionalization of the composite, resulting in lower background fluorescence. The CPI2-Cy3 was successfully quenched when bound to the BC-AuNP composite and showed no fluorescence increase when incubated with trypsin. However, after incubation in a solution containing collagenase I (Col-1), a proteinase of bacterial origin, a large fluorescence increase was observed (Figure 4.10a).

The BC-AuNP-CPI2 system was subsequently tried with two different species of bacteria, *Pseudomonas Aeruginosa* and *Staphylococcus Aureus*, which are both relevant wound infection pathogens. Live bacteria were added to the BC-AuNP-CPI2 sensor and incubated for 20 h and a large, time-dependent, fluorescence recovery was observed (Figure 4.10b).

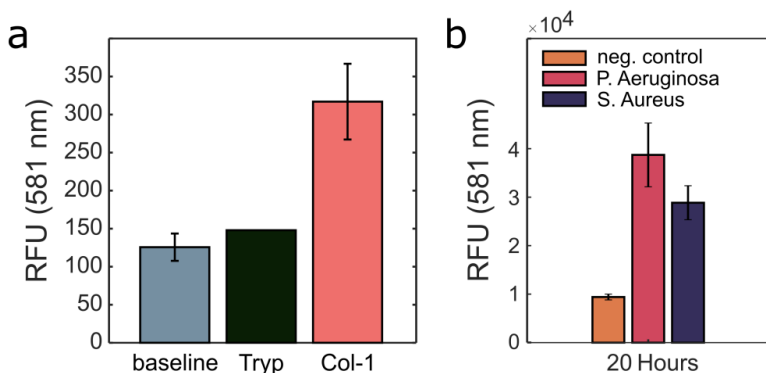


Figure 4.10: a) Fluorescence emission intensity at 581 nm after incubation of BC-AuNP-CPI2 in protease solution for 90 min. b) Fluorescence emission intensity at 581 nm after BC-AuNP-CPI2 was incubated in suspensions of live bacteria for 20 h. Error bars show standard deviations.

5

Summary of papers

This thesis includes five papers, one published and four manuscripts intended for publication. This chapter contains a summary of the included papers.

Paper I

Self-assembly of Mechanoplasmonic Bacterial Cellulose-Metal Nanoparticle Composites

Eskilson O., Lindström S.B., Sepulveda B., Shahjamali M.M., Güell-Grau P., Sivilér P., Skog M., Aronsson C., Björk E.M., Nyberg N., Khalaf H., Bengtsson T., James J., Ericson M.B., Martinsson E., Selegård R., and Aili D.

Advanced Functional Materials, **2020**, 30, 2004766

In this paper, the self-assembly process of metal NPs to BC was described and optimized. The interactions between citrate stabilized NPs and BC fibrils were elucidated and modelled, and it was shown that the process allows NPs of different geometries and compositions to be immobilized. The resulting BC-NP composites were studied for use in different applications. BC-AgNP showed antimicrobial effects. AuNP (\varnothing 50 nm) adsorbed to BC retained sharp LSPR maximum necessary for refractometric sensing and the performance of BC-AuNP (\varnothing 50 nm) were compared to standard glass substrates, showing large increase in signal-to-noise ratio. BC-AuNP (\varnothing 13 nm) were used for a proof-of-concept mechanoplasmonic biosensor utilizing the tendency for near-field interactions between closely separated metal NPs. BC with large amounts of AuNP (\varnothing 13 nm) showed significant photothermal heating due to the high absorption of light by the immobilized NPs. The heating was further increased by compression of the composites due to increasing near-field interactions resulting in enhanced light absorbance. Additionally, BC-AuNP (\varnothing 13 nm) was investigated using far-field multiphoton laser scanning microscopy showing compression induced multiphoton-induced luminescence.

Paper II

Nanocellulose Composite Wound Dressings for Real-Time pH Wound Monitoring

*Eskilson O.**, *Zattarin E.**, *Berghlund L.*, *Oksman K.*, *Hanna K.*, *Rakar J.*, *Sivlér P.*, *Skog M.*, *Rinklake I.*, *Shamasha R.*, *Sotra Z.*, *Starkenberga A.*, *Odén M.*, *Wiman E.*, *Khalaf H.*, *Bengtsson T.*, *Junker J.P.E.*, *Selegård R.*, *Björk E.M.*, and *Aili D.*

** Equal contribution*

Submitted (2023)

The aim of this paper was to design a pH-responsive wound dressing for real-time monitoring of wound pH and early detection of wound infections. The dressings were based on pure high-quality bacterial nanocellulose (BC) that was functionalized with mesoporous silica nanoparticles (MSNs) using a unique self-assembly strategy. Concentrations of adsorbed MSNs was investigated and optimized, and the specific surface area of resulting composites was analyzed using nitrogen physisorption, showing a large increase in specific surface area after the addition of MSNs. A strategy for encapsulating a pH-responsive dye, BTB, in the MSNs was developed, yielding pH-responsive wound dressings that allowed for high contrast naked-eye monitoring of wound pH with spatiotemporal resolution. Adsorption of MSNs and subsequent BTB functionalization did not have any negative effects on the function of the materials for wound dressing applications, including water vapor transmission rate and tensile strength. Compression relaxation decay was shown to decrease after adsorption of MSNs in BC, which may allow BC-MSN composites to better withstand joint compression compared to native BC. Cytocompatibility was investigated *in vitro* using human primary keratinocytes and dermal fibroblasts. Finally, *in vivo* function was successfully demonstrated in non-infected and infected porcine wounds.

Paper III

Bacterial Cellulose–Gold Nanoparticle Composite Wound Dressings for Protease Activity Monitoring

Eskilson O., Wiman E., Reustle N., Sotra Z., Svärd A., Junker J.P.E., Khalaf H., Bengtsson T., Selegård R., and Aili D.

In Manuscript (2023)

In this paper we designed wound dressings with integrated protease activity sensing capabilities for detection of wound infections. AuNPs self-assembled in BC was functionalized with fluorophore (Cy3) labeled protease substrates. The short separation between the AuNP and Cy3 resulted in fluorescence quenching. First, casein was investigated as a substrate. Addition of trypsin or collagenase type 1 resulted in an increase in fluorescence intensity due to the cleavage of casein. The increase was more pronounced for trypsin compared to Col-1. To improve the relative fluorescence increase we further explored the use of a cysteine terminated Cy3-labeled polypeptide (Cy3-CPI2-C). CPI2 is cleaved by a range of matrix metalloproteinases and bacterial proteases and was immobilized on the AuNPs via the thiol in the Cys residue. Exposure to Col-1 resulted in fluorescence turn-on. The CPI2 functionalized dressings were subsequently exposed to both culture supernatants from *S. aureus* and *P. aeruginosa* as well as live bacteria. Both of these common wound pathogens triggered a significant increase in fluorescence from the wound dressings, indicating possibilities to use these protease responsive wound dressings for rapid detection of wound infections.

Paper IV

Self-Assembled Nanocellulose–Metal Nanoparticle Composites for Catalysis

Eskilson O., Kollenchery Ramanathan S., Selegård R., and Aili D.

In Manuscript (2023)

This work examined the catalytic properties of BC functionalized with metal NPs. The adsorption to BC circumvented issues with colloidal stability while the large effective surface area of BC allowed for large numbers of NPs to be immobilized. As a model reaction, the oxidation of 4-nitrophenol by sodium borohydride was investigated using different catalytic metal NPs. Citrate stabilized AuNP, AgNPs and PtNPs were immobilized to BC and their respective catalytic efficiency was examined. In addition, the BC was dissociated to generate dispersed nanocellulose fibrils to increase accessibility to the NPs and avoid diffusion limitations. BC-AuNP composites were dissociated through ultrasonication. The improvements in mass-transfer resulted in a large increase in catalytic activity compared to intact BC-AuNP. Moreover, when BC was dissociated prior addition of AuNPs, the adsorption of the NPs to the BC fibrils turned out to be extremely fast (minutes instead of days). The catalytic rate was, however, similar when using AuNPs adsorbed to BC prior dissociation, thus revealing a new method to generate BC stabilized and highly efficient metal NP-based catalysts.

Paper V

Ultra-black Nanocellulose–Gold Nanoparticle Composites

Eskilson O., Silander J., Hallberg T.S., Åkerlind C., Järrendahl K., Selegård R. and Aili D.

In Manuscript (2023)

In this work we utilized the capacity of BC to adsorb huge amounts of AuNPs through self-assembly. The large effective surface area of nanofibrillar BC and the additional NPs formed by the adsorbed AuNPs combined with their large extinction coefficients, resulted in composite materials with very high absorptance of light over a broad wavelength range. To assess the importance of BC surface structure on the interaction of the composites with light, two different drying methods (lyophilization and air drying) of the materials were investigated and compared to hydrated BC-AuNP composites. Air-drying resulted in a very flat material with virtually zero transmittance between 250–2500 nm. Lyophilization resulted in a more porous structure where average interparticle distance was larger and consequently a slightly higher transmittance. Hydrated composites showed very high absorptance in the visible spectrum (>97%) but was rather transparent for $\lambda > 1500$ nm, whereas lyophilized and air-dried composites showed slightly lower absorptance but less transmittance. This study shows the possibility to tune optical properties of BC-AuNP composites by using the correct drying method, allowing for simple fabrication of soft and flexible broad band light absorbers.

Conclusions and future outlook

The exploration of the astonishing versatility of nanostructures, nanosystems, and nanofabrication to influence virtually every aspect of materials science has likely only started. “There is plenty of room at the bottom” was the title of Richard Feynman’s famous lecture held in 1959 on the future of nanofabrication and its implications, and even more than sixty years later, the enterprise of science still has a lot to discover in this domain.

As we enter an era where the Earth’s resources are looked upon as the finite resources they are, development of sustainable materials are becoming an increasingly large point of focus for materials science. Among such materials, cellulose may well be considered the pinnacle of sustainability due to its abundance, ease of harvesting, biodegradability, low toxicity, and high versatility. The natural and synthetic permutations of cellulose are many and they result in an impressive range of properties that will be, and are, useful for a great span of applications, a span which can surely be extended as research on cellulose is continuing. Unfortunately, many of the more

advanced applications of cellulose so far require purification of cellulose that involves harsh chemicals. Until cellulose processing has progressed to a stage where such chemicals can be excluded or minimized, BC offers a way to produce cellulose of high purity. Although BC production is miniscule in comparison to the production of pulp-based cellulose, the coming decades may see a large increase in BC production and a significant decrease in BC production costs.

Nanoparticles show properties that are useful in a vast number of applications, some of which have been mentioned in this thesis. The use of nanostructures may lead to reduced material consumption when replacing macroscale counterparts, not seldom with a concurrent increased efficiency (per weight unit), and sometimes resulting in new properties altogether.

The work presented in this thesis expands on the work on nanocellulose-NP composites by introducing a new and improved way to synthesize BC-AuNP composites in a facile fashion where control over NP morphology and composition is intact, and where NP concentration can be easily tuned. The resulting BC-NP composites have been used to improve on, or enable, materials used for such different areas as biosensing, biomedicine and catalysis, among others.

Paper I

Before commercial or research applications based on mechanoplasmonics can be realized, some fundamental aspects need to be elucidated. For instance, the way adsorbed molecules prevent near-field interactions between AuNPs needs to be better understood to be able to design a biosensor with any type of specificity. A study in which molecules of different sizes, charge, etc. are adsorbed and the resulting mechanoplasmonic response measured would be a good step forward. Furthermore, while BC has many properties useful for mechanoplasmonic sensors, it is possible that using a more homogeneous and isotropic substrate may help in understanding the underlying mechanisms of suppression of near-field interactions. Perhaps, with a highly reproducible composite, it may be possible to probe mechanical properties of adsorbed species using a mechanoplasmonic transduction strategy.

The miniaturization that is possible due to the use of LSPR based refractometric sensors in contrast to SPR based sensors, allows for the development of point-of-care

devices. In the instances that these will be optically measured using more rudimentary spectrometers, perhaps on sites where advanced laboratory instrument may be unavailable, the increase in S/N that can be accomplished by using BC-AuNP composites could be crucial for achieving a reliable signal.

Paper II

MSNs are used in drug delivery, in part due to their high specific surface area. A natural next step for BC-MSN composites could be to use MSNs for this purpose by delivering antimicrobial compounds directly to the wound site by incorporating them into the BC-MSN wound dressing. Moreover, MSNs have applications not pertaining to biomedicine that would be interesting to study in combination with BC, like adsorption of CO₂ for carbon capture technology, or water filtration.

Paper III

The capability of the sensor synthesized in **Paper III** to successfully report on bacterial protease activity *in vitro* was demonstrated. However, the *in vivo* function of the sensor still needs to be tested. Due to the complexity of the wound microenvironment and presence of proteases also in healthy wounds, it is possible that the design needs to be adjusted to successfully be able to distinguish between proteolytic activity in a healthy and an infected wound. This could involve further optimization of the peptide sequence used for protease recognition.

The tendency of proteases and proteinases to cleave a multitude of protein and peptide sequences is a problem when trying to design a highly specific protease sensor. However, the ease with which AuNPs can be functionalized may allow for the functionalization of AuNPs with an array of different polypeptide sequences conjugated with reporting molecules with different fluorescence emission spectra. With this method, it may be possible to pinpoint a specific fluorescence fingerprint to a specific species of bacteria, based on the cleaving efficiency of their proteinases, and thereby circumventing the problem of polypeptide specificity.

Paper IV

The increased NP content per unit weight of substrate that self-assembly of NPs to BC allow, can potentially lead to the development of more efficient catalytic materials. Additionally, hydrogels have been converted to aerogels or composites with maintained 3D structure after removing the solvent by different drying techniques. Such processing could enable catalysis of different gaseous compounds by directing a flow of gas through a BC-AuNP membrane.

Paper V

Broad band absorbing materials are often constructed via nanofabrication to achieve control of the material structure which is very delicate. It is likely that the structure of BC-AuNP composites can be optimized with relatively little effort by better controlling e.g., the drying techniques. Another interesting route would be to use dissociated BC-AuNP and see if it can be reassembled into a broad band absorbing material. Mixed with the proper binding material, it is possible that the dissociated BC-AuNP could be used similar to a regular paint.

References

- [1] D. Schaming, H. Remita, *Found. Chem.* **2015**, *17*, 187.
- [2] L. A. Dykman, N. G. Khlebtsov, *Acta Naturae* **2011**, *3*, 34.
- [3] F. Anthonii, *Francisci Antonii... Panacea aurea, sive, Tractatus duo de ipsius auro potabili: nunc primum in Germania ex Londinensi exemplari excusi...*; Ex Bibliopolio Frobeniano, **1618**.
- [4] J. Jeevanandam, A. Barhoum, Y. S. Chan, A. Dufresne, M. K. Danquah, *Beilstein J. Nanotechnol.* **2018**, *9*, 1050.
- [5] V. Sinkevičius, *Off. J. Eur. Union* **2022**, 65.
- [6] M. F. Hochella, D. W. Mogk, J. Ranville, I. C. Allen, G. W. Luther, L. C. Marr, B. P. McGrail, M. Murayama, N. P. Qafoku, K. M. Rosso, N. Sahai, P. A. Schroeder, P. Vikesland, P. Westerhoff, Y. Yang, *Science (80-.)*. **2019**, 363.
- [7] M. Faraday, *Philos. Trans. R. Soc. London* **1857**, *147*, 145.
- [8] G. Mie, *Ann. Phys.* **1908**, *330*, 377.
- [9] E. T. Thostenson, C. Li, T. W. Chou, *Compos. Sci. Technol.* **2005**, *65*, 491.
- [10] F. Faupel, V. Zaporozhchenko, H. Greve, U. Schürmann, V. S. K. Chakravadhanula, C. Hanisch, A. Kulkarni, A. Gerber, E. Quandt, R. Podschun, *Contrib. to Plasma Phys.* **2007**, *47*, 537.
- [11] M. H. Al-Saleh, U. Sundararaj, *Carbon N. Y.* **2009**, *47*, 2.
- [12] Y. Yang, L. Ma, J. Wu, *Mrs Bull.* **2004**, *29(11)*, 833.
- [13] C. Hanisch, A. Kulkarni, V. Zaporozhchenko, F. Faupel, *J. Phys. Conf. Ser.* **2008**, *100*, 1.
- [14] K. C. Hribar, M. H. Lee, D. Lee, J. A. Burdick, *ACS Nano* **2011**, *5*, 2948.
- [15] Y. Chen, H. Chen, J. Shi, *Adv. Mater.* **2013**, *25*, 3144.
- [16] A. Hasmann, E. Wehrschuetz-Sigl, G. Kanzler, U. Gewessler, E. Hulla, K. P. Schneider, B. Binder, M. Schintler, G. M. Guebitz, *Diagn. Microbiol. Infect. Dis.* **2011**, *71*, 12.
- [17] C. R. Loayza, D. C. S. Cardoso, D. J. A. Borges, A. A. F. Castro, A. C. Bozzi, M. A. L. Dos Reis, E. M. Braga, *Mater. Des.* **2022**, *223*, 111169.
- [18] P. Palmero, *Nanomaterials* **2015**, *5*, 656.
- [19] N. Afsarimanesh, A. Nag, M. Eshrat e Alahi, S. Sarkar, S. Mukhopadhyay, G. S. Sabet, M. E. Altinsoy, *Sensors Actuators A Phys.* **2022**, *344*, 113743.
- [20] J. W. Rhim, H. M. Park, C. S. Ha, *Prog. Polym. Sci.* **2013**, *38*, 1629.
- [21] K. Kuroda, T. Ishida, M. Haruta, *J. Mol. Catal. A Chem.* **2009**, *298*, 7.
- [22] X. Wu, C. Lu, Z. Zhou, G. Yuan, R. Xiong, X. Zhang, **2014**, 71.

- [23] M. Kaushik, A. Moores, *Green Chem.* **2016**, *18*, 622.
- [24] E. Roduner, *Chem. Soc. Rev.* **2006**, *35*, 583.
- [25] M. E. Davis, *Nature* **2002**, *417*, 813.
- [26] C. T. Kresge, M. E. Leonowicz, W. J. Roth, J. C. Vartuli, J. S. Beck, *Asian J. Chem.* **1992**, *359*, 710.
- [27] K. S. W. Sing, D. H. Everett, R. A. W. Haul, L. Moscou, R. A. Pierotti, J. Rouquérol, T. Simieniewska, *Pure Appl. Chem.* **1985**, *57*, 603.
- [28] A. Schneemann, J. L. White, S. Kang, S. Jeong, L. F. Wan, E. S. Cho, T. W. Heo, D. Prendergast, J. J. Urban, B. C. Wood, M. D. Allendorf, V. Stavila, *Chem. Rev.* **2018**, *118*, 10775.
- [29] A. Belushkin, F. Yesilkoy, J. J. González-López, J. C. Ruiz-Rodríguez, R. Ferrer, A. Fàbrega, H. Altug, *Small* **2020**, *16*, 1906108.
- [30] R. C. Hayward, P. Alberius-henning, B. F. Chmelka, G. D. Stucky, *Microporous Mesoporous Mater.* **2001**, *45*, 619.
- [31] E. M. Björk, F. Söderlind, M. Odén, *Langmuir* **2013**, *29*, 13551.
- [32] A. Rahikkala, S. A. P. Pereira, P. Figueiredo, M. L. C. Passos, A. R. T. S. Araújo, M. L. M. F. S. Saraiva, H. A. Santos, *Adv. Biosyst.* **2018**, *2*, 1.
- [33] H. T. Chen, S. Huh, J. W. Wiench, M. Pruski, V. S. Y. Lin, *J. Am. Chem. Soc.* **2005**, *127*, 13305.
- [34] M. A. A. Aziz, A. A. Jalil, S. Triwahyono, S. M. Sidik, *Appl. Catal. A Gen.* **2014**, *486*, 115.
- [35] L. Wang, H. Zhang, X. Zhou, Y. Liu, B. Lei, *J. Colloid Interface Sci.* **2016**, *478*, 256.
- [36] J. Yang, F. Cheng, Z. Zhu, J. Feng, M. Xue, Z. Meng, L. Qiu, *Analyst* **2020**, *145*, 4352.
- [37] G. T. Barnes, I. R. Gentle, *Interfacial Science: An Introduction*; Second edi.; Oxford University Press Inc., New York: New York, NY, 2011.
- [38] C. Solliard, M. Flueli, *Surf. Sci.* **1985**, *156*, 487.
- [39] O. A. Williams, J. Hees, C. Dieker, W. Jäger, L. Kirste, C. E. Nebel, *ACS Nano* **2010**, *4*, 4824.
- [40] B. Roldan Cuenya, F. Behafarid, *Surf. Sci. Rep.* **2015**, *70*, 135.
- [41] F. Viñes, J. R. B. Gomes, F. Illas, *Chem. Soc. Rev.* **2014**, *43*, 4922.
- [42] C. N. R. Rao, P. P. Edwards, *Chemistry (Easton)*. **2002**, *8*.
- [43] B. K. Pong, H. I. Elim, J. X. Chong, W. Ji, B. L. Trout, J. Y. Lee, *J. Phys. Chem. C* **2007**, *111*, 6281.
- [44] V. V. Boldyrev, *Russ. Chem. Rev.* **1973**, *42*, 515.
- [45] A. K. Galwey, G. M. Laverty, *Solid State Ionics* **1990**, *38*, 155.
- [46] N. H. Fletcher, *J. Chem. Phys.* **1958**, *29*, 572.

- [47] J. E. Millstone, W. Wei, M. R. Jones, H. Yoo, C. A. Mirkin, *Nano Lett.* **2008**, *8*, 2526.
- [48] B. Nikoobakht, M. A. El-Sayed, *Chem. Mater.* **2003**, *15*, 1957.
- [49] N. G. Bastús, J. Comenge, V. Puentes, *Langmuir* **2011**, *27*, 11098.
- [50] W. Leng, P. Pati, P. J. Vikesland, *Environ. Sci. Nano* **2015**, *2*, 440.
- [51] M. L. Personick, C. A. Mirkin, *J. Am. Chem. Soc.* **2013**, *135*, 18238.
- [52] M. Grzelczak, J. Pérez-Juste, P. Mulvaney, L. M. Liz-Marzán, *Chem. Soc. Rev.* **2008**, *37*, 1783.
- [53] J. Turkevich, P. C. Stevenson, J. Hillier, *Discuss. Faraday Soc.* **1951**, *11*, 55.
- [54] M. C. Daniel, D. Astruc, *Chem. Rev.* **2004**, *104*, 293.
- [55] J. W. Park, J. S. Shumaker-Parry, *J. Am. Chem. Soc.* **2014**, *136*, 1907.
- [56] G. Zhang, Z. Yang, W. Lu, R. Zhang, Q. Huang, M. Tian, L. Li, D. Liang, C. Li, *Biomaterials* **2009**, *30*, 1928.
- [57] P. Alexandridis, *Chem. Eng. Technol.* **2011**, *34*, 15.
- [58] K. G. Neoh, E. T. Kang, *Polym. Chem.* **2011**, *2*, 747.
- [59] L. Tian, Q. Jiang, K. K. Liu, J. Luan, R. R. Naik, S. Singamaneni, *Adv. Mater. Interfaces* **2016**, *3*, 1.
- [60] R. Fenger, E. Fertitta, H. Kirmse, A. F. Thünemann, K. Rademann, **2012**, *14*, 9343.
- [61] Y. Wang, D. Aili, R. Selegård, Y. Tay, L. Baltzer, H. Zhang, B. Liedberg, *J. Mater. Chem.* **2012**, *22*, 20368.
- [62] J. N. Israelachvili, *Intermolecular and Surface Forces: Third Edition*; 2011.
- [63] A. Lundgren, M. Hulander, J. Brorsson, M. Hermansson, H. Elwing, O. Andersson, B. Liedberg, M. Berglin, *Part. Part. Syst. Charact.* **2014**, *31*, 209.
- [64] O. Eskilson, S. B. Lindström, B. Sepulveda, M. M. Shahjamali, P. Güell-Grau, P. Sivlér, M. Skog, C. Aronsson, E. M. Björk, N. Nyberg, H. Khalaf, T. Bengtsson, J. James, M. B. Ericson, E. Martinsson, R. Selegård, D. Aili, *Adv. Funct. Mater.* **2020**, *30*, 2004766.
- [65] M.-C. Desjonquères, D. Spanjaard, *Concepts in surface physics.*; 2. ed.; Springer, 1996.
- [66] B. Liedberg, C. Nylander, I. Lundström, *Biosens. Bioelectron.* **1995**, *10*.
- [67] B. Liedberg, C. Nylander, I. Lundström, *Sensors and Actuators* **1983**, *4*, 299.
- [68] P. Englebiene, *Analyst* **1998**, *123*, 1599.
- [69] N. Nath, A. Chilkoti, *Anal. Chem.* **2004**, *76*, 5370.
- [70] M. C. Estevez, M. A. Otte, B. Sepulveda, L. M. Lechuga, *Anal. Chim. Acta* **2014**, *806*, 55.
- [71] K. A. Willets, R. P. Van Duyne, *Annu. Rev. Phys. Chem.* **2007**, *58*, 267.
- [72] V. Amendola, R. Pilot, M. Frascioni, O. M. Maragò, M. A. Iatì, *J. Phys. Condens. Matter* **2017**, *29*.

- [73] A. Dmitriev, *Nanoplasmonic Sensors*; Dmitriev, A., Ed.; 1st ed.; Springer International Publishing, 2012.
- [74] E. Martinsson, M. M. Shahjamali, K. Enander, F. Boey, C. Xue, D. Aili, B. Liedberg, *J. Phys. Chem. C* **2013**, *117*, 23148.
- [75] P. Chen, X. Liu, G. Goyal, N. T. Tran, J. C. Shing Ho, Y. Wang, D. Aili, B. Liedberg, *Anal. Chem.* **2018**, *90*, 4916.
- [76] R. Elghanian, J. J. Storhoff, R. C. Mucic, R. L. Letsinger, C. A. Mirkin, *Science (80-.)*. **1997**, *277*, 1078.
- [77] S. K. Ghosh, T. Pal, *Chem. Rev.* **2007**, *107*, 4797.
- [78] L. Jauffred, A. Samadi, H. Klingberg, P. M. Bendix, L. B. Oddershede, *Chem. Rev.* **2019**, *119*, 8087.
- [79] G. Baffou, R. Quidant, *Laser Photonics Rev.* **2013**, *7*, 171.
- [80] D. Tordera, D. Zhao, A. V. Volkov, X. Crispin, M. P. Jonsson, *Nano Lett.* **2017**, *17*, 3145.
- [81] K. Bae, G. Kang, S. K. Cho, W. Park, K. Kim, W. J. Padilla, *Nat. Commun.* **2015**, *6*.
- [82] J. N. Armor, *Catal. Today* **2011**, *163*, 3.
- [83] W. A. Herrmann, B. Cornils, *Angew. Chemie - Int. Ed.* **1997**, *36*, 1048.
- [84] D. J. Cole-Hamilton, *Science (80-.)*. **2003**, *299*, 1702.
- [85] L. Liu, A. Corma, *Chem. Rev.* **2018**, *118*, 4981.
- [86] M. Sankar, Q. He, R. V. Engel, M. A. Sainna, A. J. Logsdail, A. Roldan, D. J. Willock, N. Agarwal, C. J. Kiely, G. J. Hutchings, *Chem. Rev.* **2020**, *120*, 3890.
- [87] M. Haruta, *Chem. Rec.* **2003**, *3*, 75.
- [88] S. Galvagno, G. Parravano, *J. Catal.* **1978**, *55*, 178.
- [89] G. N. Vayssilov, Y. Lykhach, A. Migani, T. Staudt, G. P. Petrova, N. Tsud, T. Skála, A. Bruix, F. Illas, K. C. Prince, V. Matolín, K. M. Neyman, J. Libuda, *Nat. Mater.* **2011**, *10*, 310.
- [90] M. Haruta, N. Yamada, T. Kobayashi, S. Iijima, *J. Catal.* **1989**, *115*, 301.
- [91] T. Ishida, M. Haruta, *Angew. Chemie - Int. Ed.* **2007**, *46*, 7154.
- [92] F. Shi, Y. Deng, *J. Catal.* **2002**, *211*, 548.
- [93] M. Chen, H. Kang, Y. Gong, J. Guo, H. Zhang, R. Liu, *ACS Appl. Mater. Interfaces* **2015**, *7*, 21717.
- [94] N. Nath, A. Chilkoti, *Anal. Chem.* **2002**, *74*, 504.
- [95] A. N. Shipway, E. Katz, I. Willner, *ChemPhysChem* **2000**, *1*, 18.
- [96] T. Tran, O. Eskilson, F. Mayer, R. Gustavsson, R. Selegård, I. Lundström, C. F. Mandenius, E. Martinsson, D. Aili, *Processes* **2020**, *8*, 1.
- [97] L. J. Sherry, S.-H. Chang, G. C. Schatz, R. P. Van Duyne, B. J. Wiley, Y. Xia, *Nano Lett.*

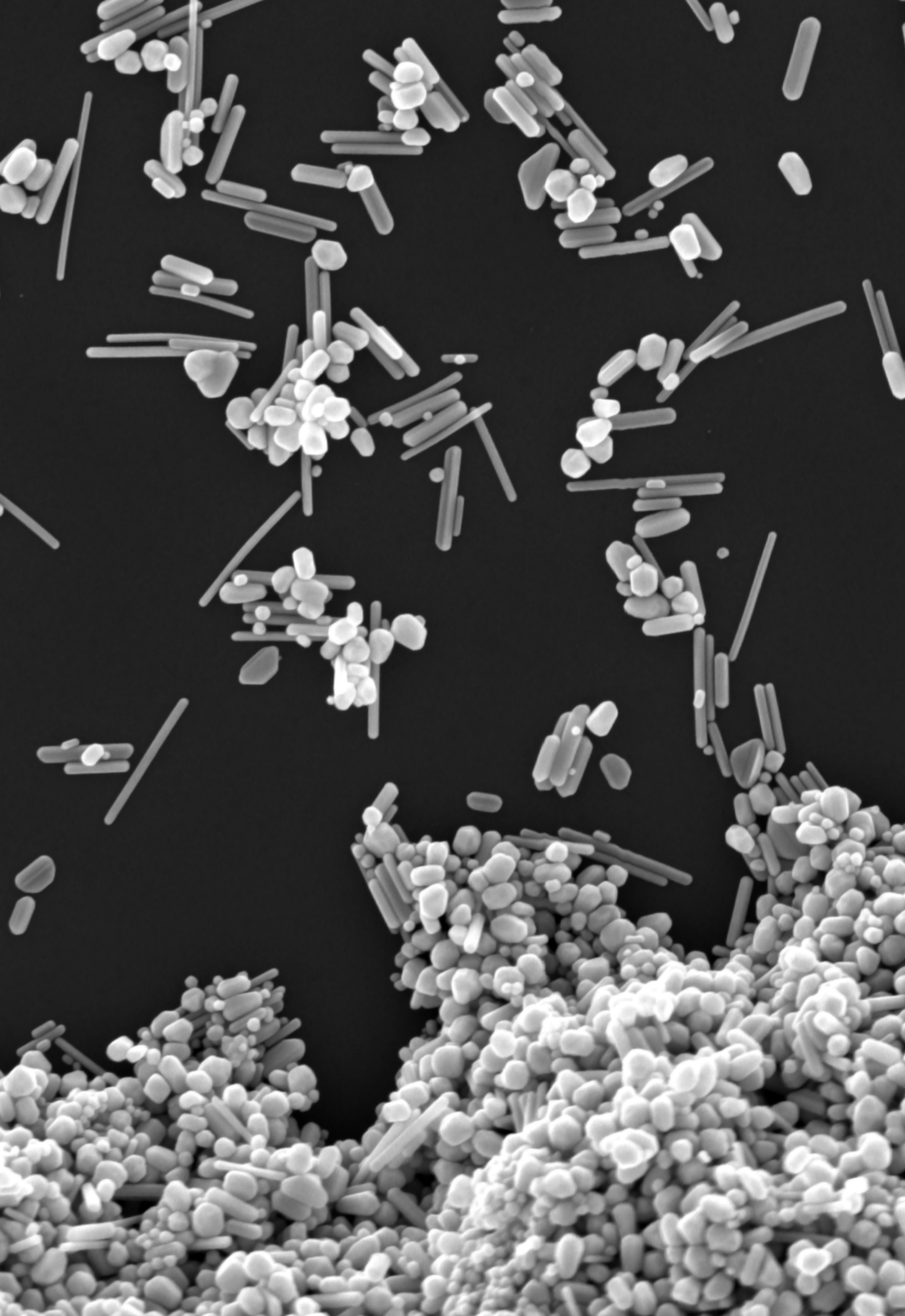
2005, *5*, 2034.

- [98] E. Martinsson, M. M. Shahjamali, N. Large, N. Zaree, Y. Zhou, G. C. Schatz, C. A. Mirkin, D. Aili, *Small* **2016**, *12*, 330.
- [99] L. J. Sherry, R. Jin, C. A. Mirkin, G. C. Schatz, R. P. Van Duyne, *Nano Lett.* **2006**, *6*, 2060.
- [100] X. Y. Zhang, A. Hu, T. Zhang, W. Lei, X. J. Xue, Y. Zhou, W. W. Duley, *ACS Nano* **2011**, *5*, 9082.
- [101] K. C. Grabar, M. B. Hommer, M. J. Natan, R. G. Freeman, *Anal. Chem.* **1995**, *67*, 735.
- [102] A. D. McFarland, R. P. Van Duyne, *Nano Lett.* **2003**, *3*, 1057.
- [103] A. N. Shipway, E. Katz, I. Willner, *Angew. Chemie (International Ed. English)* **2000**, *39*, 19.
- [104] K. Y. Lee, D. J. Mooney, *Prog. Polym. Sci.* **2012**, *37*, 106.
- [105] C. K. S. Pillai, W. Paul, C. P. Sharma, *Prog. Polym. Sci.* **2009**, *34*, 641.
- [106] M. Dash, F. Chiellini, R. M. Ottenbrite, E. Chiellini, *Prog. Polym. Sci.* **2011**, *36*, 981.
- [107] N. Lin, A. Dufresne, *Eur. Polym. J.* **2014**, *59*, 302.
- [108] D. Klemm, D. Schumann, U. Udhardt, S. Marsch, *Prog. Polym. Sci.* **2001**, *26*, 1561.
- [109] T. H. Tan, H. V. Lee, W. A. Yehya Dabdawb, S. B. B. O. A. A. Hamid, In *Materials for Biomedical Engineering: Nanomaterials-based Drug Delivery*; Elsevier, 2019; pp. 131–164.
- [110] R. J. Moon, A. Martini, J. Nairn, J. Simonsen, J. Youngblood, *Cellulose nanomaterials review: Structure, properties and nanocomposites*; 2011; Vol. 40.
- [111] D. Klemm, B. Heublein, H. P. Fink, A. Bohn, *Angew. Chemie - Int. Ed.* **2005**, *44*, 3358.
- [112] Y. Nishiyama, **2017**.
- [113] M. Wohler, T. Benselfelt, L. Wågberg, I. Furó, L. A. Berglund, J. Wohler, *Cellulose* **2022**, *29*, 1.
- [114] Y. Nishiyama, G. P. Johnson, A. D. French, V. T. Forsyth, P. Langan, *Biomacromolecules* **2008**, *9*, 3133.
- [115] Y. Habibi, L. A. Lucia, O. J. Rojas, *Chem. Rev.* **2010**, *110*, 3479.
- [116] M. Nogi, S. Iwamoto, A. N. Nakagaito, H. Yano, *Adv. Mater.* **2009**, *21*, 1595.
- [117] M. Iguchi, S. YAMANAKA Ajinomoto Central Research, J. A. Budhiono, .
- [118] H. Yano, J. Sugiyama, A. N. Nakagaito, M. Nogi, T. Matsuura, M. Hikita, K. Handa, *Adv. Mater.* **2005**, *17*, 153.
- [119] A. N. Nakagaito, M. Nogi, H. Yano, *Mrs Bull.* **2010**, *35*, 214.
- [120] A. F. Jozala, L. C. de Lencastre-Novaes, A. M. Lopes, V. de Carvalho Santos-Ebinuma, P. G. Mazzola, A. Pessoa-Jr, D. Grotto, M. Gerenutti, M. V. Chaud, *Appl. Microbiol. Biotechnol.* **2016**, *100*, 2063.

- [121] W. Tang, S. Jia, Y. Jia, H. Yang, *World J. Microbiol. Biotechnol.* **2010**, *26*, 125.
- [122] D. Y. Kim, Y. Nishiyama, S. Kuga, *Cellulose* **2002**, *9*, 361.
- [123] L. Yue, Y. Xie, Y. Zheng, W. He, S. Guo, Y. Sun, T. Zhang, S. Liu, *Compos. Sci. Technol.* **2017**, *145*, 122.
- [124] C. Huang, H. Ji, Y. Yang, B. Guo, L. Luo, Z. Meng, L. Fan, J. Xu, *Carbohydr. Polym.* **2020**, *230*, 115570.
- [125] C. N. Wu, S. C. Fuh, S. P. Lin, Y. Y. Lin, H. Y. Chen, J. M. Liu, K. C. Cheng, *Biomacromolecules* **2018**, *19*, 544.
- [126] F. A. Faisul Aris, F. N. A. Mohd Fauzi, W. Y. Tong, S. S. Syed Abdullah, *Biocatal. Agric. Biotechnol.* **2019**, *21*, 101332.
- [127] X. Wen, Y. Zheng, J. Wu, L. Yue, C. Wang, J. Luan, Z. Wu, K. Wang, *Prog. Nat. Sci. Mater. Int.* **2015**, *25*, 197.
- [128] J. L. Clement, P. S. Jarrett, *Met. Based. Drugs* **1994**, *1*, 467.
- [129] T. Maneerung, S. Tokura, R. Rujiravanit, *Carbohydr. Polym.* **2008**, *72*, 1.
- [130] G. Yang, Y. Yao, C. Wang, *Mater. Lett.* **2017**, *209*, 11.
- [131] L. C. de Santa Maria, A. L. C. Santos, P. C. Oliveira, H. S. Barud, Y. Messaddeq, S. J. L. Ribeiro, *Mater. Lett.* **2009**, *63*, 797.
- [132] M. Karlsson, P. Olofsson, I. Steinvall, F. Sjöberg, J. Thorfinn, M. Elmasry, *Adv. Wound Care* **2019**, *8*, 71.
- [133] G. delli Santi, A. Borgognone, *Burn. Open* **2019**, *3*, 103.
- [134] G. Han, R. Ceilley, *Adv. Ther.* **2017**, *34*, 599.
- [135] G. Gethin, S. Cowman, D. N. Kolbach, *Cochrane Database Syst. Rev.* **2015**, *2017*, CD008599.
- [136] R. Portela, C. R. Leal, P. L. Almeida, R. G. Sobral, *Microb. Biotechnol.* **2019**, *12*, 586.
- [137] T. Sivilér, P. Sivilér, M. Skog, L. Conti, D. Aili, *Adv. Ski. Wound Care* **2018**, *31*, 306.
- [138] L. Zheng, S. Li, J. Luo, X. Wang, *Front. Bioeng. Biotechnol.* **2020**, *8*, 1.
- [139] M. S. Brown, B. Ashley, A. Koh, *Front. Bioeng. Biotechnol.* **2018**, *6*, 1.
- [140] L. A. Schneider, A. Korber, S. Grabbe, J. Dissemond, *Arch. Dermatol. Res.* **2007**, *298*, 413.
- [141] I. A. I. Wilson, M. Henry, R. D. Quill, P. J. Byrne, *Vasa - J. Vasc. Dis.* **1979**, *8*, 339.
- [142] B. Mirani, E. Pagan, B. Currie, M. A. Siddiqui, R. Hosseinzadeh, P. Mostafalu, Y. S. Zhang, A. Ghahary, M. Akbari, *Adv. Healthc. Mater.* **2017**, *6*, 1.
- [143] C. Gamerith, D. Luschnig, A. Ortner, N. Pietrzik, J. H. Guse, M. Burnet, M. Haalboom, J. van der Palen, A. Heinzle, E. Sigl, G. M. Gübitz, *Sensors Actuators, B Chem.* **2019**, *301*, 126966.
- [144] L. Liu, X. Li, M. Nagao, A. L. Elias, R. Narain, H.-J. Chung, *Polymers (Basel)*. **2017**, *9*, 558.

- [145] A. Tamayol, M. Akbari, Y. Zilberman, M. Comotto, E. Lesha, L. Serex, S. Bagherifard, Y. Chen, G. Fu, S. K. Ameri, W. Ruan, E. L. Miller, M. R. Dokmeci, S. Sonkusale, A. Khademhosseini, *Adv. Healthc. Mater.* **2016**, *5*, 711.
- [146] N. Pan, J. Qin, P. Feng, Z. Li, B. Song, *J. Mater. Chem. B* **2019**, *7*, 2626.
- [147] R. Rahimi, M. Ochoa, T. Parupudi, X. Zhao, I. K. Yazdi, M. R. Dokmeci, A. Tamayol, A. Khademhosseini, B. Ziaie, *Sensors Actuators, B Chem.* **2016**, *229*, 609.
- [148] D. A. Jankowska, M. B. Bannwarth, C. Schulenburg, G. Faccio, K. Maniura-Weber, R. M. Rossi, L. Scherer, M. Richter, L. F. Boesel, *Biosens. Bioelectron.* **2017**, *87*, 312.
- [149] C. Zhou, N. Tang, X. Zhang, Y. Fang, Y. Jiang, H. Zhang, X. Duan, *Front. Chem.* **2020**, *8*, 194.
- [150] H. Charaya, T.-G. La, J. Rieger, H.-J. Chung, *Adv. Mater. Technol.* **2019**, *4*, 1900327.
- [151] P. Martin, R. Nunan, *Br. J. Dermatol.* **2015**, *173*, 370.
- [152] R. Serra, R. Grande, L. Butrico, A. Rossi, U. F. Settimio, B. Caroleo, B. Amato, L. Gallelli, S. De Franciscis, *Expert Rev. Anti. Infect. Ther.* **2015**, *13*, 605.
- [153] M. T. Tran, A. Kumar, A. Sachan, M. Castro, W. Allegre, J. F. Feller, *Chemosensors* **2022**, *10*.
- [154] D. Yu, Y. Chen, C. C. Ahrens, Y. Wang, Z. Ding, H. Lim, C. Fell, K. P. Rumbaugh, J. Wu, W. Li, *Analyst* **2020**, *145*, 8050.
- [155] E. Morales-Narváez, H. Golmohammadi, T. Naghdi, H. Yousefi, U. Kostiv, D. Horák, N. Pourreza, A. Merkoçi, *ACS Nano* **2015**, *9*, 7296.
- [156] R. J. B. Pinto, P. A. A. P. Marques, M. A. Martins, C. P. Neto, T. Trindade, *J. Colloid Interface Sci.* **2007**, *312*, 506.
- [157] E. Martinsson, B. Sepulveda, P. Chen, A. Elfving, B. Liedberg, D. Aili, *Plasmonics* **2014**, *9*, 773.
- [158] T. Zhang, W. Wang, D. Zhang, X. Zhang, M. Yurong, Y. Zhou, L. Qi, *Adv. Funct. Mater.* **2010**, *20*, 1152.
- [159] L. Tian, J. Luan, K. K. Liu, Q. Jiang, S. Tadepalli, M. K. Gupta, R. R. Naik, S. Singamaneni, *Nano Lett.* **2016**, *16*, 609.
- [160] D. Mirska, K. Schirmer, S. S. Funari, A. Langner, B. Dobner, G. Brezesinski, *Colloids Surfaces B Biointerfaces* **2005**, *40*, 51.
- [161] B. Isomaa, J. Reuter, B. M. Djupsund, *Arch. Toxicol.* **1976**, *35*, 91.
- [162] J. Wan, J. H. Wang, T. Liu, Z. Xie, X. F. Yu, W. Li, *Sci. Rep.* **2015**, *5*, 1.
- [163] E. E. Connor, J. Mwamuka, A. Gole, C. J. Murphy, M. D. Wyatt, *Small* **2005**, *1*, 325.
- [164] C. Carnovale, G. Bryant, R. Shukla, V. Bansal, *ACS Omega* **2019**, *4*, 242.
- [165] K. H. Su, Q. H. Wei, X. Zhang, J. J. Mock, D. R. Smith, S. Schultz, *Nano Lett.* **2003**, *3*, 1087.
- [166] N. J. Halas, S. Lal, W. S. Chang, S. Link, P. Nordlander, *Chem. Rev.* **2011**, *111*, 3913.

- [167] P. K. Jain, W. Huang, M. A. El-Sayed, *Nano Lett.* **2007**, 7, 2080.
- [168] D. E. McCoy, T. Feo, T. A. Harvey, R. O. Prum, *Nat. Commun.* **2018**, 9, 1.
- [169] H. Tao, J. Lin, Z. Hao, X. Gao, X. Song, C. Sun, X. Tan, *Appl. Phys. Lett.* **2012**, 100, 1.
- [170] C. Ng, L. W. Yap, A. Roberts, W. Cheng, D. E. Gómez, *Adv. Funct. Mater.* **2017**, 27.
- [171] N. Kwon, H. Oh, R. Kim, A. Sinha, J. Kim, J. Shin, J. W. M. Chon, B. Lim, *Nano Lett.* **2018**, 18, 5927.
- [172] Y. Hu, K. Cao, H. Rong, J. Xu, H. Han, H. Wang, L. Pattelli, N. Li, H. Xu, J. Zhao, L. Pan, A. Kuchmizhak, Y. Li, *ACS Appl. Nano Mater.* **2021**, 4, 7995.
- [173] J. Q. Xi, M. F. Schubert, J. K. Kim, E. F. Schubert, M. Chen, S. Y. Lin, W. Liu, J. A. Smart, *Nat. Photonics* **2007**, 1, 176.
- [174] H. Hosoda, H. Mori, N. Sogoshi, A. Nagasawa, S. Nakabayashi, *J. Phys. Chem. A* **2004**, 108, 1461.
- [175] I. Niskanen, T. Suopajärvi, H. Liimatainen, T. Fabritius, R. Heikkilä, G. Thungström, *J. Quant. Spectrosc. Radiat. Transf.* **2019**, 235, 1.
- [176] P. Paximada, E. A. Dimitrakopoulou, E. Tsouko, A. A. Koutinas, C. Fasseas, I. G. Mandala, *Carbohydr. Polym.* **2016**, 150, 5.
- [177] P. C. S. F. Tischer, M. R. Sierakowski, H. Westfahl, C. A. Tischer, *Biomacromolecules* **2010**, 11, 1217.
- [178] A. Svärd, J. Neilands, E. Palm, G. Svensäter, T. Bengtsson, D. Aili, **2020**, 3, 9822.



Papers

The papers associated with this thesis have been removed for copyright reasons. For more details about these see:

<https://doi.org/10.3384/9789180750622>

FACULTY OF SCIENCE AND ENGINEERING

Linköping Studies in Science and Technology, Dissertations No. 2292, 2023
Department of Physics, Chemistry and Biology (IFM)

Linköping University
SE-581 83 Linköping, Sweden

www.liu.se